Electric Motor Systems
Platform EMSA

Testing industrial silicon carbide Variable Speed Drives

October 2025

Technology Collaboration Programme
by IEA

Electric Motor Systems Platform – 2025

The report was prepared under the IEA Technology Collaboration Programme on Energy Efficient End-Use Equipment (4E) – **Electric Motor Systems Platform** (EMSA).

Authors:

Prof. Dr Andrea Vezzini, Bern University of Applied Sciences, Switzerland

Thomas Lanz, Bern University of Applied Sciences, Switzerland

Abstract:

The investigation of silicon carbide (SiC) Variable Speed Drives (VSDs) shows promising increases in efficiency through higher switching frequencies, but only up to a certain point. While the reduction of the current harmonics reduces motor losses, the switching losses of the VSD dominate if the switching frequencies are too high, so that the overall efficiency drops again.

The investigations into partial discharge effects on the windings (PD) have confirmed that SiC VSDs can generate higher overvoltages at motor connections due to steeper voltage edges. This can lead to accelerated ageing of the winding insulation, especially if existing VSDs are replaced without adjustments. An increase in bearing currents has also been observed, although the effects of this depend heavily on the bearing type and operating conditions.

Despite the theoretical advantages of SiC technology, the long-term tests revealed problems with the reliability of the available VSDs, which justifies further research into the robustness and industrial applicability of wide bandgap (WBG) semiconductors. The development of a comprehensive research roadmap represents an important step towards clarifying open questions regarding the introduction and optimisation of WBG technologies in industrial drives.

This report is an extract of the German report ‘EMSA-IS&T: IEA 4E EMSA Task International Standards and Testing’ published on 30 November 2024 (SFOE contract number SI/501851-01, link to original report: https://www.aramis.admin.ch/Texte/?ProjectID=43471&Sprache=en-US).

Figure on report cover: 5.5 kW silicon carbide Variable Speed Drive on the Bern University of Applied Sciences (BFH) 10 kW test bench. Source: BFH, 2023.

About the IEA 4E Electric Motor Systems Platform (EMSA):

The goal of the Electric Motor Systems Platform EMSA is to increase energy efficiency and reduce greenhouse gas emissions worldwide by promoting highly efficient electric motor systems in the EMSA member countries, industrialised countries, emerging economies and developing countries. Electric motor systems were responsible for more than 50% of the global electric energy consumption in 2023.

Further information on EMSA is available at: www.iea-4e.org/emsa

About the IEA Technology Collaboration Programme on Energy Efficient End-Use Equipment (4E TCP):

The Technology Collaboration Programme on Energy Efficient End-Use Equipment (4E TCP), has been supporting governments to coordinate effective energy efficiency policies since 2008. Fourteen countries and one region have joined together under the 4E TCP platform to exchange technical and policy information focused on increasing the production and trade in efficient end-use equipment. However, the 4E TCP is more than a forum for sharing information: it pools resources and expertise on a wide range of projects designed to meet the policy needs of participating governments. Members of 4E find this an efficient use of scarce funds which results in outcomes that are far more comprehensive and authoritative than can be achieved by individual jurisdictions. The 4E TCP is established under the auspices of the International Energy Agency (IEA) as a functionally and legally autonomous body.

Current members of 4E TCP are: Australia, Austria, Canada, China, Denmark, European Commission, France, Japan, Korea, Netherlands, New Zealand, Switzerland, Sweden, United Kingdom and the United States.

The main collaborative research and development activities under 4E include the

- Electric Motor Systems Platform (EMSA)
- Efficient, Demand Flexible Networked Appliances (EDNA) Platform
- Smart Sustainability in Lighting and Controls (SSLC) Platform
- Power Electronic Conversion Technology Platform (PECTA)

Further information on the 4E TCP is available from: www.iea-4e.org

Disclaimer

The Technology Collaboration Programme on Energy Efficient End-Use Equipment (4E TCP) Electric Motor Systems Platform (EMSA) has made its best endeavours to ensure the accuracy and reliability of the data used herein, however makes no warranties as to the accuracy of data herein, nor accepts any liability for any action taken or decision made based on the contents of this report.

Views, findings and publications of the 4E TCP do not necessarily represent the views or policies of the IEA Secretariat or its individual member countries.

Translation note

This report is an extract of the German report ‘EMSA-IS&T: IEA 4E EMSA Task International Standards and Testing’ published on 30 November 2024. This report was translated from the original language with the assistance of ChatGPT into English following which it has been carefully reviewed. All content, including figures, interpretations and conclusions, originates exclusively from the authors.

Table of contents

List of abbreviations

ACEE	Advisory Committee on Energy Efficiency
BFH	Bern University of Applied Sciences
CENELEC	European Committee for Electrotechnical Standardisation
EMC	Electromagnetic compatibility
EMSA	Electric Motor Systems Platform
GaN	Gallium Nitride
IEA	International Energy Agency
IEC	International Electrotechnical Commission
MEPS	Minimum Energy Performance Standards
MTBF	mean-time-between-failure
NC	National Committee
PD	Partial Discharge
PDIV	Partial Discharge Inception Voltage
RPDIV	Repetitive Partial Discharge Inception Voltage
RR'C	Round Robin Converters (Round Robin Variable Speed Drives)
SC	IEC Technical Subcommittees
SFOE	Swiss Federal Office of Energy
Si	Silicon
SiC	Silicon carbide
TC	Technical Committee
TCP	IEA Technology Collaboration Programme
VSD	Variable Speed Drive
WG	Working Group

Summary

The investigation of silicon carbide (SiC) VSDs shows promising efficiency gains at higher switching frequencies, but only up to a certain limit. While reducing current harmonics lowers motor losses, excessive switching frequencies cause VSD switching losses to dominate, ultimately reducing overall efficiency.

Studies on partial discharge (PD) effects in windings confirm that SiC VSDs can produce higher overvoltage at motor terminals due to faster voltage rise rates. This can accelerate the ageing of winding insulation, particularly when existing VSDs are replaced without corresponding motor-side adjustments. Increased bearing currents have also been observed, though their impact strongly depends on bearing type and operating conditions.

Despite the theoretical benefits of SiC technology, long-term tests have revealed reliability issues in currently available VSDs. This highlights the need for further research into the robustness and industrial suitability of wide-bandgap (WBG) semiconductors. Developing a comprehensive research roadmap is therefore a crucial step toward resolving open questions surrounding the adoption and optimisation of WBG technologies in industrial drives.

Key take-aways

- Silicon carbide (SiC) VSDs can improve overall efficiency through higher switching speeds, which reduce motor losses. However, the switching frequency must be carefully matched to the motor. Excessively high switching frequencies can lead to a decline in overall efficiency.
- The fast voltage rise times of SiC VSDs can cause overvoltages at the motor terminals. This is particularly critical when replacing VSDs on older motors whose insulation systems are not designed for such stress. An increase in bearing currents has also been observed, although whether this is harmful depends strongly on the bearing type and operating conditions. A general conclusion cannot be drawn.

1. Introduction

As part of the IEA 4E Electric Motor Systems Platform, Switzerland — represented by Andrea Vezzini — assumes a co-leadership role in the two work packages “International Standards” and “International Motor Systems Testing.” These two work packages represent the principal focal areas within the Electric Motor Systems Platform.

Within the work package “International Motor Systems Testing,” the activity “SiC VSDs for Industrial Drives” (March 2021–April 2024) investigated the influence of high switching speeds of silicon carbide (SiC) devices on the ageing behaviour of electrical machine windings.

The ultra-fast voltage transients (dV/dt) inherent to SiC power semiconductor switches subject both the electrical insulation system (EIS) and the motor bearings to significant electrical stress. Such stress has been shown to accelerate ageing processes, potentially resulting in premature insulation breakdown or bearing damage. In the dedicated “SiC VSD Test Series” subproject, the insulation condition was evaluated through partial discharge (PD) measurements in electrical machine windings, while a complementary methodology for detecting bearing degradation is currently under development and validation.

Despite their documented advantages, the industrial adoption of wide-bandgap (WBG) semiconductors, including SiC and Gallium Nitride (GaN), continues to face several challenges. The most frequently cited concerns relate to cost and long-term reliability, increased system complexity, and potential risks to equipment during retrofitting or integration. To address these issues, the “Wide-Bandgap Power Semiconductor Industrial VSD Research Roadmap” subproject (2024–2027) has been elaborated in collaboration with national research groups in Switzerland and several international partners. This initiative is expected to culminate in the publication of a “White Book,” which will provide strategic guidance for the deployment, standardization, and optimisation of WBG technologies in industrial drive applications.

2. Motivation of the project

2.1. Sub-project SiC inverter test series

Silicon carbide (SiC) VSDs provide superior efficiency compared to conventional silicon-based VSDs. This improvement is primarily attributed to their substantially lower conduction and switching losses, as well as the reduced reverse recovery charge of SiC devices. Consequently, SiC technology enables higher switching capacities and requires less energy during the turn-on and turn-off phases.

The reduced thermal losses of SiC VSDs also permit simplified or even passive cooling solutions, which contribute to reductions in system volume, weight, and infrastructure costs. Furthermore, the capability to operate at elevated switching frequencies results in lower motor current harmonics, thereby decreasing additional harmonic losses in the connected electrical machines.

Nevertheless, the ultra-fast voltage transients (dV/dt) inherent to SiC components impose significant electrical stress on the motor's electrical insulation system (EIS). This stress accelerates ageing mechanisms and can ultimately lead to premature insulation failure. The insulation condition can be monitored through partial discharge (PD) measurements in electrical machine windings, with experimental investigations demonstrating that the steepness of the applied voltage slope is a decisive parameter influencing EIS lifetime.

In addition, pulse-width modulated (PWM) VSDs are recognized as a major contributor to bearing failures in VSD-fed motor drive systems. All VSD topologies generate common-mode voltages with respect to ground, which couple through parasitic capacitances between the stator winding and rotor. This induces bearing currents that flow from the rotor to the grounded stator housing. Such currents may result in the decomposition of lubricating grease or localized melting of the bearing raceways due to electrical discharge machining (EDM), both of which compromise bearing reliability and shorten service life.

2.2. Sub-project Wide Bandgap Power Semiconductor Industrial VSD Research Roadmap

VSDs based on wide-bandgap (WBG) semiconductors such as SiC and GaN offer significantly higher efficiency compared to conventional silicon-based VSDs. This improvement is mainly due to substantially lower conduction and switching losses, as well as the drastically reduced reverse recovery charge during turn-on and turn-off transitions. Moreover, the reduced heat generation of WBG devices allows for smaller cooling systems, thereby lowering space requirements, weight, and overall infrastructure costs in industrial VSD applications.

Another key advantage is the ability to operate at higher switching frequencies, which reduces motor current harmonics. This not only lowers harmonic losses in electrical machines but also enhances overall system performance and efficiency. The superior thermal properties and electrical behaviour of WBG devices further support longer device lifetimes and improved reliability, making them highly attractive for industrial drive systems. Importantly, extended lifetime also contributes to sustainability and, at least partially, to circular-economy principles by keeping products and materials in use for longer periods.
In summary, WBG semiconductors enable a range of benefits in industrial drives: higher efficiency, reduced cooling requirements, more compact designs, and enhanced reliability. Together, these advantages lower operating costs while improving performance, positioning WBG devices as a compelling choice for modern industrial applications.

3. Testing project objectives

3.1. Project objectives of the SiC VSD test series sub-project

Three results are expected from the SiC VSD test series:

1. **Baseline performance comparison**
   Establish a baseline for several key performance parameters of the VSD (CDM) and the complete power drive system (PDS). Where possible, tests should be conducted in accordance with existing standards. The objective is to evaluate whether SiC VSDs can be measured with sufficient accuracy using current standards and measurement devices.

2. **Impact on electrical insulation system (EIS)**
   Building on the results of the literature review, a dedicated test programme will be developed to assess the influence of SiC VSDs on the ageing of the electrical insulation system. At least two test systems will be set up (SiC-based and Si-based, ideally also including a three-level setup). Since partial discharges (PD) are both a symptom and, in some cases, a cause of insulation deterioration in motor and generator stator windings, PD behaviour will be closely monitored. Where feasible, online PD measurements will be implemented; otherwise, periodic offline tests will be scheduled.

3. **Investigation of motor bearing currents (optional)**
   As an additional objective, the feasibility of using the same test setup to measure motor bearing currents —and thereby investigate potential bearing failures— will be explored.

3.2. Project objectives of the WBG-Power Semiconductor Industrial VSD Research Roadmap sub-project

Two results are expected from the Wide Bandgap Power Semiconductor Industrial VSD Research Roadmap:

1. **Critical analysis of current challenges**
   Although wide-bandgap semiconductors (SiC and GaN) offer numerous advantages, their introduction into industrial applications still faces several challenges and points of criticism. The roadmap will identify the most frequently cited arguments against widespread adoption, explain them, and assess their validity.

2. **Formulation of research questions**
   Based on this analysis, targeted research questions will be developed to address industry concerns. The aim is to provide evidence that can refute these objections and thereby accelerate the adoption of wide-bandgap power semiconductors in industrial VSDs.

4. System description

BFH set up a new test rig in phase 2 to investigate insulation ageing. It had to be considered that several fault patterns may occur as the insulation deteriorates. Figure 1 illustrates the stator locations where partial discharges are most likely to arise.

A breakdown can occur:

- between the windings of two phases (“phase-to-phase”),
- within a single winding of a phase (“turn-to-turn”), or
- between the winding of a phase and the housing (“phase-to-ground”).

Depending on the fault location, different diagnostic methods must be applied. Partial discharge (PD) activity manifests as microcurrent disturbances, which are difficult to detect under normal operating conditions. In the laboratory, however, the use of resistance and impulse testers allows controlled application of voltages with defined waveforms, enabling accurate measurement of PD levels and the partial discharge inception voltage (PDIV).

Fig.2 Locations with a high risk of partial discharge

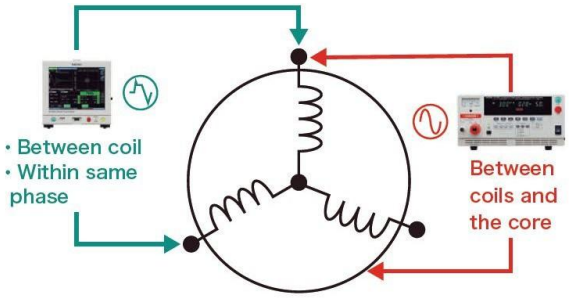

Fig.3 Test voltage when connected to the neutral point

Figure 1 and Figure 2: Impulse voltage tester vs. withstand voltage tester

If the stator is connected at the neutral point in a star configuration, insulation failures between two phases or within a single phase can only be detected by applying a surge voltage (Figure 2).

In contrast, insulation between the windings and the housing (earth) can be tested using a high AC voltage, as supplied by a withstand voltage tester.

Figure 3 shows the measurement setup with the impulse measuring device (right) and the withstand voltage tester (left). Both instruments, together with the memory measuring device and the high-frequency current probe, were provided by HIOKI. A high-voltage differential probe from Micsig was additionally employed to capture the high surge voltages.

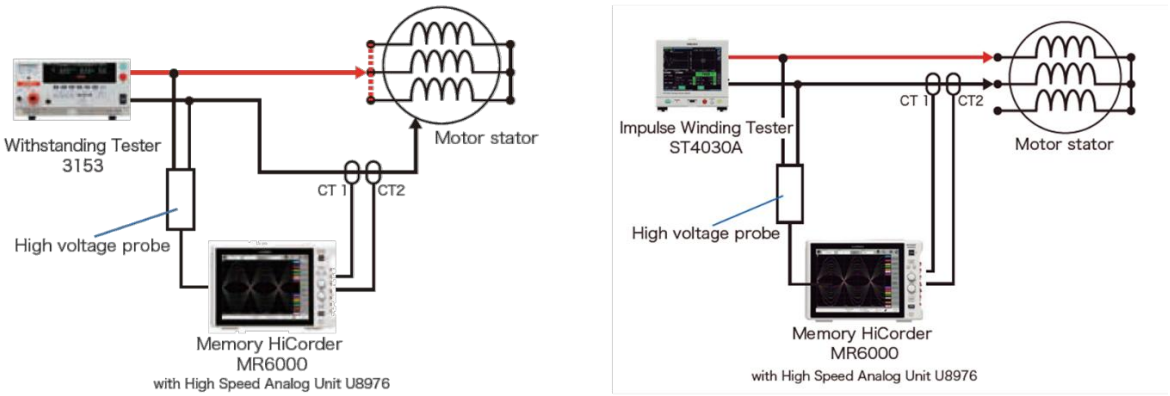

Figure 3: Monitoring the state of health of the windings using periodic partial discharge tests; phase-to-earth PD test using continuous high voltage (left) and phase-to-phase PD test using HV pulses

Table 1: Instruments for partial discharge testing

TE measuring instruments		
Oscilloscope	HIOKI MR6000	up to 200 MS/s
High-voltage probe head	Micsig 20003	up to 5.6 kV, 100 MHz
Current probe	HIOKI CT6711	3 measuring ranges, up to 30 Arms, 120 MHz
Pulse voltage tester	HIOKI ST4030A	up to 4.2 kV
Withstand voltage tester	HIOKI 3153	up to 5 kVrms AC/DC

As described in the literature review, the waveform and rise time of the applied voltage have a significant influence on PD activity. It is therefore important to note that partial discharge behaviour emulated in the laboratory does not necessarily correspond to its location or intensity under real operating conditions if the excitation voltage differs. Nevertheless, insulation ageing can still be compared with laboratory measurements, with the pulse voltage test providing a closer approximation to the conditions encountered in operation with PWM VSDs, and thus being the preferred method.

5. Procedure and method

"SiC VSD test series"

1. **Baseline performance comparison**
   Establish a baseline for several key performance parameters of the VSD (CDM) and the complete power-driven system (PDS). Where possible, tests will be conducted in accordance with existing standards.
2. **Impact on electrical insulation system (EIS)**
   Based on the study results, a dedicated test programme will be developed to evaluate the influence of the SiC VSD on insulation ageing. At least two test systems will be set up (SiC-based and Si-based). Partial discharges (PD) are both a symptom and, in some cases, a cause of various insulation degradation mechanisms in motor and generator stator windings. The feasibility of online PD measurement will be investigated; if not viable, periodic offline tests will be scheduled.
3. **Investigation of motor bearing currents (optional)**
   As an additional objective, it will be examined whether the same test setup can also be used to measure motor bearing currents, thereby enabling the detection of bearing-related failures. If not feasible, the motors will be supplemented with a dedicated bearing current measurement device.

"Wide Bandgap Power Semiconductor Industrial VSD Research Roadmap"

1. **Definition of objectives**
   Define the objective of the research roadmap based on a catalogue of arguments currently raised against the use of wide-bandgap (WBG) VSDs.
2. **Formulation of research questions**
   Organise a workshop with key stakeholders in the Swiss research community to formulate targeted research questions aimed at accelerating the development and industrial adoption of WBG VSDs.

6. Work carried out

"Testing: SiC VSD test series"

With the LARA-100k, PERUN Technologies offers an open-platform VSD featuring a SiC-based output stage with a rated power of 5.5 kW. The core of the PERUN system is the main board with the TI C2000 plug-in microcontroller, which provides connectivity to either an industrial or a dedicated PERUN SiC power stage, as well as to the PERUN expansion board (communication, GPIO) and the PERUN PowerDesk software. At the time of the test design, this was the only industrial VSD with SiC technology available on the market. However, the official PERUN website (link) still does not list the VSD as a standard product.

The two VSDs delivered to the Bern University of Applied Sciences —after a waiting period of more than a year— carry the serial numbers 001 and 002. Not surprisingly, several issues were encountered during commissioning and during the planned long-term tests.

6.1. System tests

The efficiency tests are conducted in accordance with IEC 61800-9-2. Both VSDs are tested at different switching frequencies to evaluate the expected advantages of SiC components on system efficiency at higher switching frequencies.

While higher switching frequencies reduce motor losses by lowering current harmonics, they simultaneously increase VSD switching losses. Therefore, only measurements of the complete drive system can provide meaningful information about overall efficiency.

The efficiency measurements are performed using two PW6001 master/slave power analysers from HIOKI. Several operating points with varying VSD load factors are tested at different switching frequencies, as specified in Table 2 and illustrated in Figure 4.

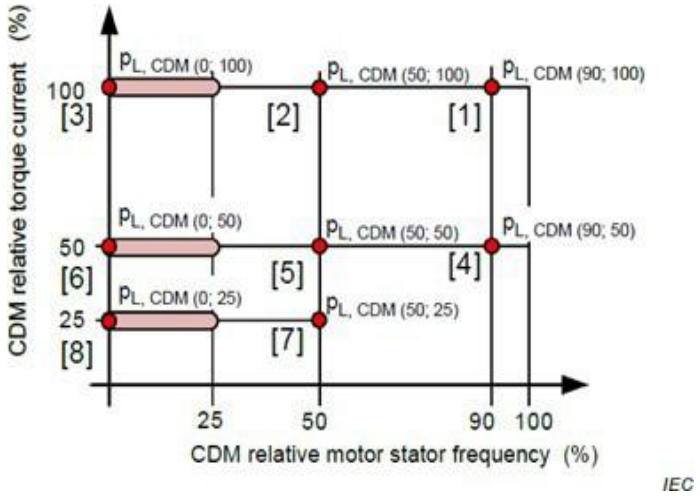

Figure 4: *Test points used in accordance with IEC61800-9-2*

Table 2: *Switching frequency settings for efficiency tests in the range of the two VSD capacities*

Tested switching frequencies (kHz)	
ATV930*	4, 10, 16
LARA-100k**	4, 10, 16, 40, 70, 100

* ATV930= Schneider Electric ATV930U55N4

** LARA-100k= PERUN LARA-100k

6.2. Partial discharge tests

To investigate the fault characteristics reported in the literature —such as partial discharge and bearing damage— under operation with a SiC VSD, a dedicated test setup was designed for comparative ageing tests on induction machines. Two identical brand-new general-purpose machines, each rated at 4 kW, were mechanically coupled. One machine was operated by a standard regenerative industrial VSD, while the other was driven by a wide-bandgap (WBG) VSD.

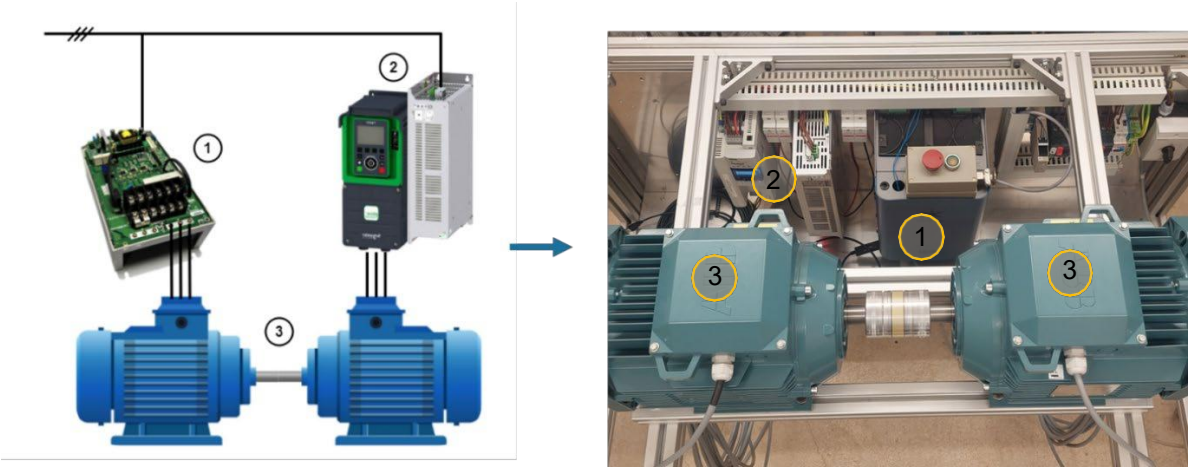

Figure 5: Overview of the specified test setup with 1) SiC VSD (Perun LARA-100k) 2) Industrial VSD (Lenze i550) and regenerative unit 3) Coupled induction machines.

6.3. Test procedure and results

The test campaign was structured into four steps:

1. Preliminary measurements – including VSD setup, verification of VSD behaviour, and PWM characterisation.
2. Efficiency testing – of the VSD, the electrical machines, and the complete drive system.
3. Initial machine characterisation – including measurement of the partial discharge inception voltage (PDIV) and all parameters to be monitored during ageing.
4. Long-term operation – including periodic inspections.

While steps 1–3 were completed successfully (after resolving some initial commissioning issues), significant problems arose during the planned long-term endurance tests in step 4. After approximately 100 operating hours, the LARA-100k VSD exhibited abnormal behaviour, randomly switching to error mode without apparent cause and shutting down. By reducing the load and continuously monitoring its status, a further 200 operating hours were achieved (300 hours in total) before the VSD failed completely.

The defective VSD was returned for repair, while the second unit was commissioned to investigate possible causes of the malfunction. The manufacturer later confirmed that the first VSD had entered the fault state due to a partially defective MOSFET. Assuming this was an isolated case, long-term testing was resumed with the second VSD. However, within less than 24 hours this unit also exhibited comparable failures and ultimately broke down.

Following its repair, the first VSD was briefly reused for bearing-current measurements but failed again after a short operating period when subjected to endurance testing. In total, three VSD failures occurred—two with brand-new units and one after repair—which forced the cancellation of the endurance test due to time constraints and the absence of a viable SiC alternative.

Given that the test application represents a standard industrial use case (as underlined by the trouble-free operation of the Si-based reference VSD), the recurring failures suggest a fundamental reliability issue of the LARA-100k in this context. Since the endurance tests could not be completed, additional efforts were redirected towards an in-depth literature review on partial discharge phenomena in motor windings under SiC VSD operation. Furthermore, the most important findings from the first 300 hours, as well as the general procedure for insulation condition assessment, are presented in this report.

6.4. Bearing current measurement

To enable reliable measurement of bearing currents without altering the motors used in the endurance test, an additional motor of the same type was modified specifically for this purpose. This approach also eliminated motor-related measurement deviations, ensuring more consistent comparative results between operation with the Si-based and SiC-based VSDs.

For the modification, the motor was dismantled and two Rogowski coils (type CWT MiniHF 015) were installed inside the housing, positioned directly in front of the bearings. Mounting was made possible using existing holes in the bearing shells and newly fabricated brackets. The measuring cables were routed outside the housing via dedicated feed-throughs, allowing the motor to be operated under near-original conditions.

The Rogowski coils employed offer a bandwidth of 150 Hz to 23 MHz and a high sensitivity of 200 mV/A. With the chosen arrangement, circular currents of identical polarity could be

measured. In addition, a contact brush was used to measure the bearing voltage i.e., the potential difference between the motor shaft and the motor housing.

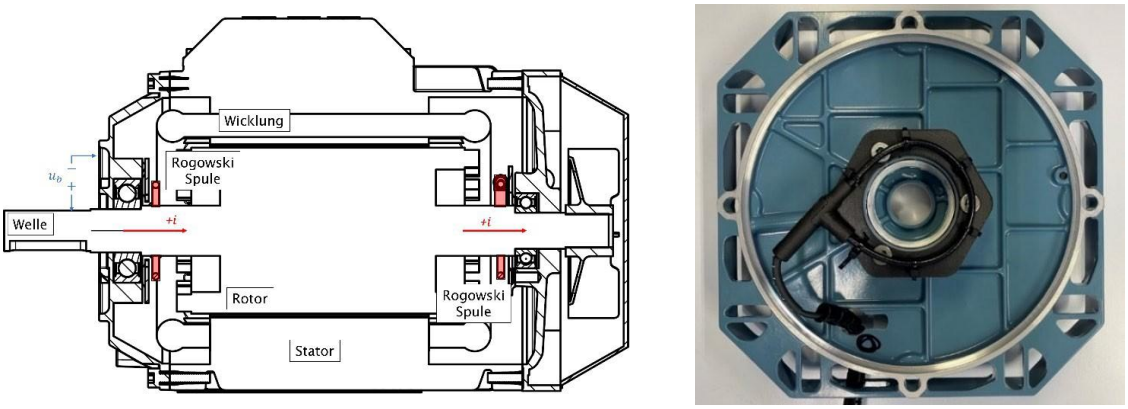

Figure 6: Position and measuring direction of the installed Rogowski coils as well as a detailed view of the installation of the Rogowski coil on the rear bearing shell.

6.5. "Wide Bandgap Power Semiconductor Industrial VSD Research Roadmap"

On 15 May 2024, a workshop was held at BFH in Bern with key stakeholders from the Swiss scientific community (UAS and ETH). The purpose was to discuss a background paper prepared by Roland Brüniger and Andrea Vezzini and to present current and planned research activities.

The background paper outlined the open questions surrounding the use of wide-bandgap (WBG) VSDs in industry and proposed possible research directions. During the workshop, relevant research projects for the period 2024–2027 were collected and evaluated. The outcome was the “Wide Bandgap Power Semiconductor Industrial VSD Research Roadmap.”

The following key challenges were identified:

- High initial investment costs

  The higher upfront cost of WBG VSDs can be a barrier to adoption, particularly in cost-sensitive applications. A detailed analysis of efficiency gains and total life-cycle costs —including SiC and GaN— could demonstrate that energy savings, especially in partial-load operation, significantly offset the higher initial investment.

- Application maturity and availability

  According to PECTA’s application readiness map, a major limitation is the restricted production capacity and availability of WBG components compared to silicon-based alternatives. This constraint may create supply-chain challenges for industries requiring large volumes of these devices.

- Complexity of system design and implementation

  Developing WBG VSDs necessitates revisiting established system designs, including VSD topologies (two-level vs. multi-level), gate-driver circuits, protection circuits, input and output filtering, and thermal management. The requirement for specialised design expertise and the added system complexity may deter some manufacturers and users.

- Reliability and longevity concerns

Although SiC and GaN devices offer superior efficiency and improved thermal and electrical performance, their long-term reliability in harsh industrial environments (continuous duty, dust, and dirt) remains a concern. Compared with silicon technology, the lack of extensive long-term field data raises additional uncertainty.

- Equipment-related risks

  Higher switching frequencies enabled by WBG devices provide many advantages but also introduce risks for connected equipment. In particular, fast voltage transients (dv/dt) can impose additional stress on motor insulation systems, bearings, and cabling, potentially reducing service life.

The WBG Industrial VSD Research Roadmap is designed to serve as a planning and coordination instrument for contributions to the forthcoming White Book on Wide Bandgap Semiconductors for Industrial Drives. It compiles details of ongoing and planned research activities, with a particular emphasis on applied and economic aspects of WBG VSD deployment in industrial applications.

7. Results of SiC VSD test series

7.1. System tests

The efficiency tests conducted on the PERUN LARA and Altivar VSDs show that the SiC-based VSD achieves significantly higher efficiency than the SI-based VSD as soon as the switching frequency is increased (Figure 8, right). However, it is also evident that a switching frequency of 100 kHz—possible with the LARA VSD—lead to excessively high losses and therefore low efficiencies from both the VSD and system perspective (Figure 8, left).

At low switching frequencies, both VSDs achieve similar efficiencies. Notably, however, the SiC VSD exhibits poorer efficiency under partial-load operation (Figure 8, right). This result contrasts with the theoretical calculations[1] (Figure 7) and suggests that the LARA VSD has an unusually high auxiliary power consumption.

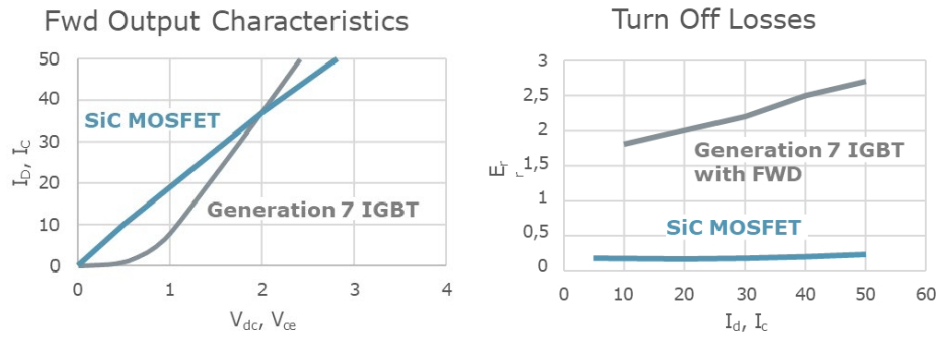

Figure 7: *Lower voltage drops in the partial load range for SiC semiconductors (conduction losses on the left) and low switch-off losses (on the right) should lead to lower efficiency losses and energy savings in the partial load range (calculated values, source:* Semikron Danfoss).

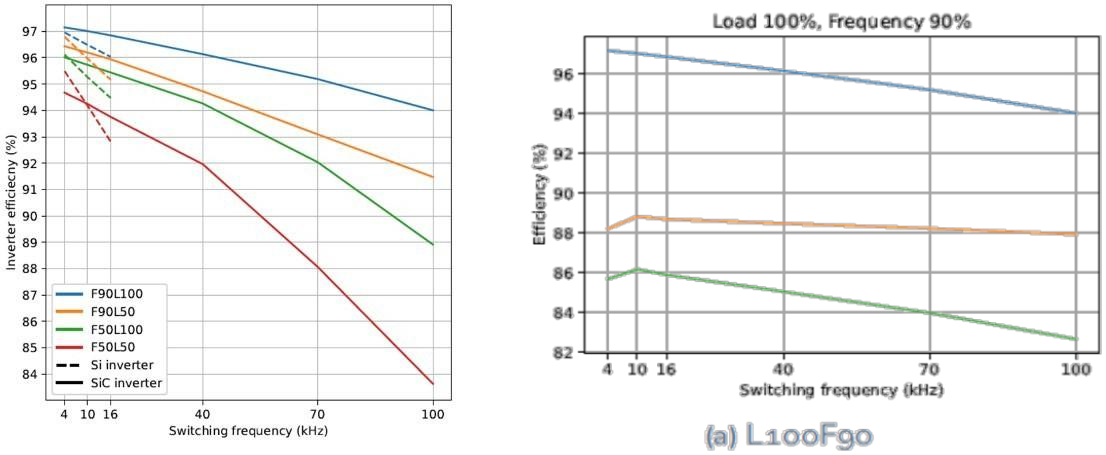

Figure 8: *Measurement results of the LARA **SiC VSD** show in the **graph on the left** a lower efficiency at partial load (orange and red fully drawn curves) at a lower switching frequency than the Schneider Si VSD (orange and red dashed line). **The graph on the right** shows an increase in the overall efficiency of the drive system (green line) at a higher switching frequency (from 4 to 10 kHz) due to the improved efficiency of the motor (orange line). The SiC VSD efficiency decreases linearly (blue line)*

[1] Webinar: Silicon Carbide in AC Motor Drives; Semikron Danfoss, https://youtu.be/RrRQ0FpnjyQ?t=564

According to the literature, the overall efficiency of the drive system (VSD and motor) initially increases with higher switching frequencies, as the reduced output current harmonics result in lower motor losses. However, once the switching frequency is raised beyond a certain point, VSD switching losses begin to dominate, while motor efficiency no longer improves. As a result, the overall efficiency decreases again.

For the specific case of a 50 Hz industrial induction motor, increasing the switching frequency above 10 kHz with the SiC VSD does not provide any further efficiency benefits for the system (Figure 8).

7.2. Basics of partial discharge tests

The pulsed control of the VSD (PWM or SV-PWM) can cause overvoltages at the terminals of a motor driven by a VSD. These overvoltages arise from wave reflections in the motor windings. The two decisive factors are the cable length between the VSD and the motor, and the voltage rise rate (dv/dt).

The following equation provides an estimate of the resulting overvoltages. It defines a critical cable length above which an applied voltage pulse may lead to a voltage doubling at the motor terminals due to wave propagation and reflection.

$$l_c = \frac{t_r v}{2}$$

With l_c denoting the critical cable length, t_r the rise time of the voltage edge, and v the propagation speed of the signal in the cable (approx. 150 m/µs):

- If the actual cable length is significantly shorter than l_c, no major overvoltages are expected.
- If the cable length exceeds l_c , overvoltage of up to twice the applied DC-link voltage may occur.
- The exact magnitude of the overvoltage additionally depends on factors such as the impedance mismatch between the cable and the motor winding.

Under typical conditions, the maximum voltage should not exceed twice the DC-link voltage[2]. However, some studies report even higher values—caused, for example, by **double pulses**[3] or by **antiresonance effects**[4], which can lead to an increased neutral-point voltage.

In the present measurements, rise times of 30 ns for the SiC VSD and 80 ns for the Silicon VSD result in critical cable lengths of approximately 2.25 m and 6 m, respectively. With a 1.7 m cable—shorter than the critical cable length for both VSDs—measured overvoltages still reached up to 1.1 kV for the SiC VSD and 750 V for the Si VSD (Figure 9). Such elevated voltages can induce partial discharges and significantly reduce the lifetime of the machine

[2] Shan Yin, King Jet Tseng, Rejeki Simanjorang, Yong Liu, and Josep Pou. A 50-kW High-Frequency and High-Efficiency SiC Voltage Source Inverter for More Electric Aircraft. IEEE TRANSACTIONS ON INDUSTRIAL ELECTRONICS, 64(11), 2017

[3] R. J. Kerkman, D. Leggate, D. Schlegel and G. Skibinski, "PWM inverters and their influence on motor overvoltage," *Proceedings of APEC 97 - Applied Power Electronics Conference*, Atlanta, GA, USA, 1997, pp. 103-113 vol.1, doi: 10.1109/APEC.1997.581440.

[4] S. Sundeep, J. Wang, A. Griffo and F. Alvarez-Gonzalez, "Antiresonance Phenomenon and Peak Voltage Stress Within PWM Inverter Fed Stator Winding," in *IEEE Transactions on Industrial Electronics*, vol. 68, no. 12, pp. 11826-11836, Dec. 2021

insulation system.

This effect is particularly relevant when replacing a silicon VSD with a silicon carbide VSD: a cable length that was previously uncritical may suddenly become problematic, subjecting the motor to much higher electrical stress than anticipated.

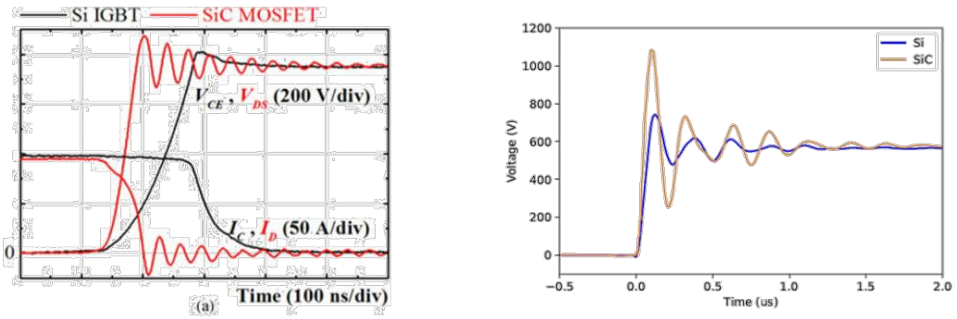

Figure 9: *Steeper switching edges generate higher overvoltage for cable lengths close to the critical cable length. Left: measurements from a publication, right: comparative measurement from the BFH laboratory; measurements with 1.7 m cable.*

However, if cables longer than the critical length for silicon VSDs (> 5–10 m) are used — which is often the case in practice and is also reflected in the standard for VSD loss measurements specifying a 15 m connection cable— the same maximum voltage peaks occur with both VSD types. This was also confirmed experimentally. In such cases, the ageing of the insulation due to partial discharges is not expected to differ significantly between the two VSD types. Nevertheless, the PD characteristics and the resulting damage are strongly influenced by the different rise times.

For this reason, the test setup at Bern University of Applied Sciences employed a 15 m long, shielded cable to investigate this effect in detail. The Partial Discharge Inception Voltage (PDIV) is considered the primary parameter for monitoring the insulation condition. The planned long-term tests are therefore intended to demonstrate how PDIV correlates with actual insulation ageing and how it is influenced by different test conditions (rise time, waveform, AC or pulse excitation).

7.3. Literature review

Because it was not possible to complete our own long-term test, we reviewed additional studies addressing the effect of the fast voltage transients of SiC VSDs on insulation lifetime. Particular attention was given to why partial discharge (PD) damage may differ under the same voltage amplitude but with different rise times.

One study[5] investigated the influence of SiC VSD rise times on motor insulation. Nine motor test specimens were subjected to different DC-link voltages (600, 800, and 1000 V), switching frequencies (20, 40, and 60 kHz), and rise times (20, 40, and 60 ns). To accelerate ageing, the motors were tested without rotors and operated at an elevated temperature of 230 °C. A mathematical model was then applied to separate thermal ageing from electrical ageing. However, doubts remain regarding the reliability of this approach, since the high temperature itself likely affects electrical ageing mechanisms, for example by altering PD behaviour. The results at nominal voltage (600 V) were also inconsistent. For instance, the greatest electrical

[5] D. Hewitt, S. Sundeep, J. Wang, A. Griffo, M. Diab and X. Yuan, "An Experimental Assessment of the Impact of High dv/dt SiC Converters on Insulation Lifetime of Electrical Machines," 2022 IEEE Energy Conversion Congress and Exposition (ECCE), Detroit, MI, USA, 2022, pp. 1-8

ageing was observed at the lowest PWM frequency and the longest rise time—contradicting current assumptions about ageing causes, but possibly attributable to manufacturing tolerances in the windings. The authors ultimately concluded that DC-link voltage is the primary factor determining PD occurrence, while PWM frequency is the second most important driver of ageing..

Even before the advent of WBG devices, several studies had examined the influence of rise time, polarity, pulse intervals, and frequency on PD behaviour and insulation degradation. Two such studies[6],[7]. investigated rise times ranging from 40 ns to 100 ns and from 50 ns to 16 µs, with frequencies of 20 kHz and 1–5 kHz, respectively. Despite differences in methodology, both reached the same conclusion: **shorter rise times and higher switching frequencies are particularly damaging to insulation.** Interestingly, one study noted that the damaging effect increased significantly below a rise time of 70 ns—approximately the boundary between the faster SiC MOSFETs and the slower Si MOSFETs.

A considerable body of literature also focuses on the origin, characterisation, and mitigation of overvoltages. One notable contribution specifically differentiates between overvoltages below 2 pu, overvoltages above 2 pu, and corresponding mitigation techniques.

From the perspective of **Partial Discharge (PD) theory**, several key mechanisms can be highlighted:

- **Ignition delay:** A free starting electron is required for PD initiation. In intact insulation, this electron must first be released, for example by a high applied electric field. During this ignition delay, if the applied voltage rises quickly, the voltage may exceed the PDIV, resulting in a higher-energy discharge once ignition occurs.
- **Energy distribution:** With slow voltage rise times, multiple low-energy PDs are likely to occur. In contrast, with fast rise times, a single discharge with higher energy is more probable.
- **Space charge effects:** After a PD event, the resulting space charge distribution counteracts the applied field. Before another PD can occur, this space charge must dissipate—a process strongly dependent on the conductivity of the insulation and thus on temperature. For this reason, rapidly repeating pulses are not always more damaging, as space charge can inhibit PD ignition.
- **Pulse polarity:** Space charge dynamics also explain the differing PD behaviour observed under unipolar and bipolar excitation.

In summary, although numerous studies have investigated insulation ageing on test specimens or developed models of overvoltage behaviour, **practical investigations into the insulation lifetime of motors operated with industrial VSDs remain scarce.**

[6] Weijun Yin, "Failure mechanism of winding insulations in inverter-fed motors," in IEEE Electrical Insulation Magazine, vol. 13, no. 6, pp. 18-23, Nov.-Dec. 1997

[7] P. Wang, A. Cavallini and G. C. Montanari, "The influence of repetitive square wave voltage parameters on enamelled wire endurance," in IEEE Transactions on Dielectrics and Electrical Insulation, vol. 21, no. 3, pp. 1276-1284, June 2014

8. Measurement results

The measurement results are presented in three sections. The first section characterises the PWM signals measured from both VSDs. The second section explains the PD measurements and the determination of the PDIV. Finally, the third section discusses the preliminary findings on insulation ageing.

8.1. PWM characterisation

The SiC-based PERUN LARA-100k VSD and the Si-based Lenze i550 VSD were used for the service-life test. A comparison of the phase-to-phase voltages during a switching event is shown in Figure 10. Owing to the 15 m cable length, the differences in overvoltage are less pronounced than with shorter cables. On average, the overvoltage measured was 1090 V for the SiC VSD and 1030 V for the Si VSD, at an intermediate DC-link voltage of 580 V.

The phase-to-earth voltages reached peak values of 780 V for the SiC VSD and 680 V for the motor driven by the Si output stage. The measured slew rates of the SiC VSD were 30 ns (≈18,000 V/µs) and 80 ns (≈6,750 V/µs), determined between 10% and 90% of Vdc (i.e., approximately 60 V to 540 V).

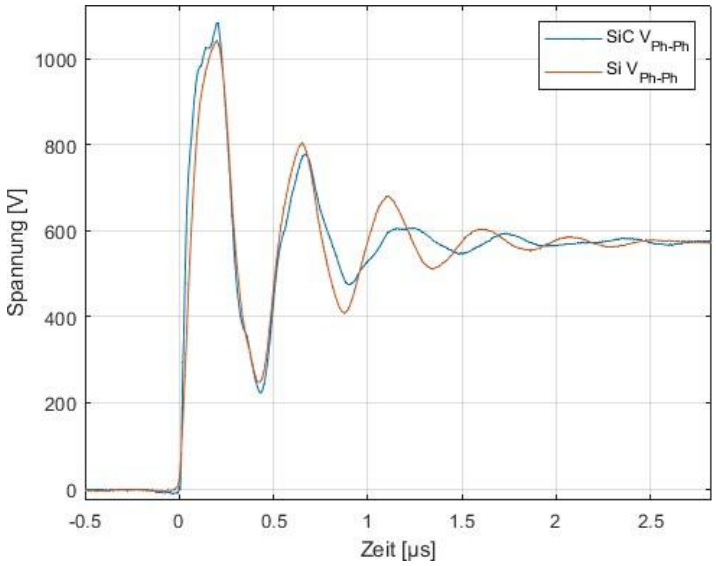

Figure 10: Comparison of the phase-to-phase voltage, measured at the motor terminals, when controlled with the SiC and Si VSD and 15 m cable length.

It is important to ensure that the motor frequency is not set above approximately 38 Hz during the endurance test; otherwise, the Lenze VSD operates in overmodulation. In this mode, the phase voltages remain at +Vdc or 0 V for certain intervals without switching. By contrast, the LARA VSD, which employs space vector PWM (SVPWM), does not enter overmodulation up to much higher frequencies. As a result, the applied switching patterns would differ between the two VSDs, potentially affecting the ageing behaviour of the insulation.

8.2. Partial discharge test (PD test)

One approach to analysing insulation ageing is to measure the **Partial Discharge Inception Voltage (PDIV)**, which decreases as ageing progresses. However, because partial discharges in motors can occur at different locations and require different test methods, the question arises as to which method is best suited for detecting ageing.

According to **DIN EN 60034-18-41**, a distinction is made between PD testing at mains frequency and at impulse voltage:

- **Mains-frequency test (50 Hz):**
  A sinusoidal voltage at 50 Hz is applied. The amplitude can either be increased stepwise to determine the PDIV, or set to the maximum available test voltage for a simple pass/fail assessment. PDIV is defined as the test voltage at which at least one partial discharge per cycle (20 ms) is detected and is specified in Vrms. This method can be used with an open neutral point for phase-to-phase testing, or with a closed neutral point for phase-to-earth testing.
- **Impulse-voltage test (surge test):**
  In this method, voltage impulses are applied and the **Repetitive Partial Discharge Inception Voltage (RPDIV)** is typically determined. The pulse voltage (defined as Vpp) is gradually increased, and a fixed number of pulses per voltage step (often 10) is applied. While the PDIV —the first voltage at which a PD occurs— can vary significantly due to the stochastic nature of PD events, the RPDIV is defined as the test voltage at which a PD occurs in at least five pulses (or ≥50% for more/less than 10 pulses). This reduces measurement variability. The impulse-voltage method can be applied for both phase-to-phase and phase-to-earth testing, even with a closed neutral point. In general, it is regarded as more representative of actual motor operation under VSD supply.

In our measurements, the rise time of the pulse tester depended on the test object and was approximately 200 ns for the motors under investigation.

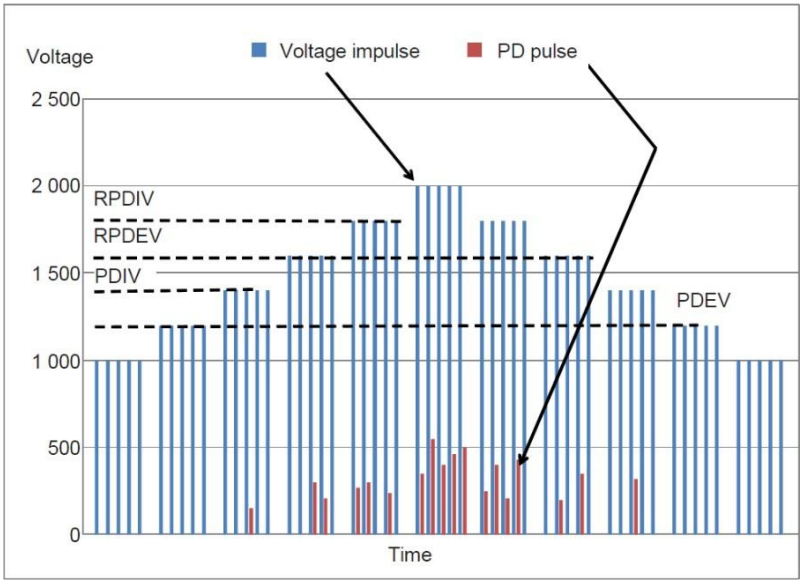

Figure 11: Method for determining PDIV (inception voltage), RPDIV (repetitive inception voltage) and the drop-out voltages according to IEC 61934.

Various PD detection methods can be applied independently of the test voltage. In this work, both voltage and current were measured and recorded during each test, with subsequent analysis performed in Python. For current-based detection, the absolute values of the measured current (the polarity of the peak being irrelevant) were high-pass filtered to isolate PD-related disturbances. A 6th-order high-pass filter was used, with a cut-off frequency of 2 MHz for measurements at mains frequency and 50 MHz for pulse tests. The filtered signals were then analysed for current peaks, with any peak exceeding 3.5 mA classified as a PD event.

The same filtering approach can in principle be applied to the voltage signal. In our measurements, however, the voltage traces exhibited greater noise, making it more difficult to reliably distinguish PD events from background interference.

Typical PD measurements are shown in Figure 12 and Figure 13.

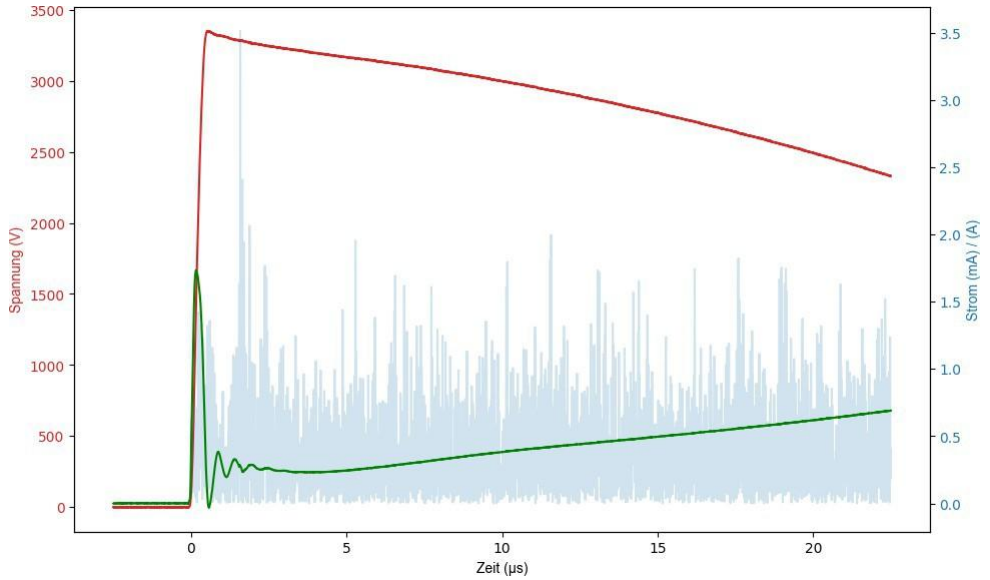

Figure 12: Current (green) and voltage curve (red) during a pulse test. The filtered current signal, which has a low-intensity PD of 3.5 mA, is shown in blue. The PD cannot be recognized in the unfiltered signal.

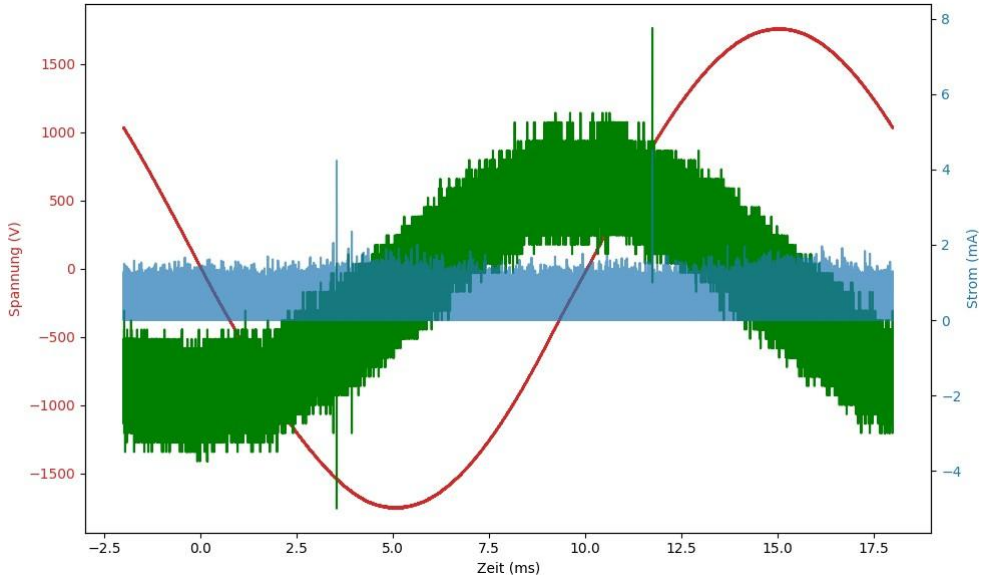

Figure 13: Current (green) and voltage curve (red) during a withstand voltage test at 50 Hz. Only low capacitive currents flow during a withstand voltage test because the neutral point is open or a phase-to-earth test is being carried out. Two PDs with low intensity can be recognized.

8.3. Measurement configurations

There are several possible motor connection configurations for the tests.

- **Pulse tests:** The motor can be connected in “Open,” “Star,” or “Delta” configuration. For each configuration, the pulse tester can be connected to the individual phases in different ways, resulting in nine possible setups.
- **Withstand voltage tests:** The measurements can be performed either with all phases connected simultaneously in “Delta” against earth, with individual phases measured against earth, or with phases measured individually against each other. This results in seven possible setups.

An overview of the connection options is provided in Figure 14.

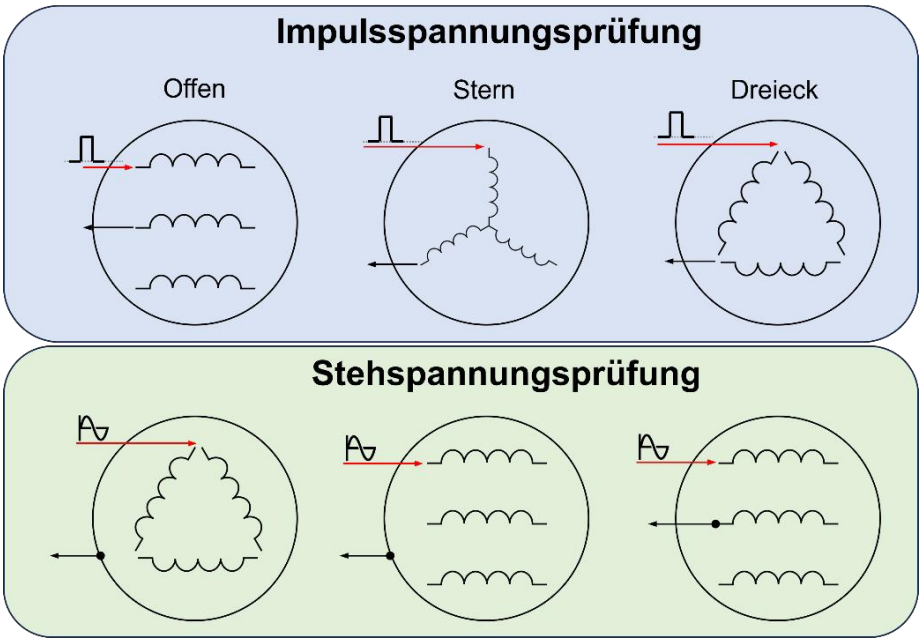

Figure 14: Connection options for impulse (in blue) and withstand (in green) voltage tests.

The large number of possible measurement configurations requires considerable effort. Therefore, once sufficient measurements had been carried out, the focus shifted to identifying which configuration is best suited for assessing insulation ageing. For this purpose, the PD probability —defined as the ratio of PD-generating pulses to the total number of applied pulses— was plotted for the three configurations (“open,” “star,” and “delta”), as shown in Figure 15. The evaluation includes the measurement data of both motors operated with the Si and SiC VSDs.

The results show that PD occurs only rarely (<10%) below 2 kV, while the probability increases most rapidly for the “delta” configuration. This can be explained by the fact that in this setup the full impulse voltage appears across one winding as well as across the parallel-connected windings, subjecting a larger portion of the motor to the test voltage and thereby increasing PD activity. By contrast, the “open” configuration can help identify which specific winding exhibits insulation weakness, but this was not the primary aim of the present work.

For assessing the **overall insulation condition**, the “delta” configuration is sufficient. This approach also offers the practical advantage that the test motor is already wired in delta, meaning that no additional rewiring is required.

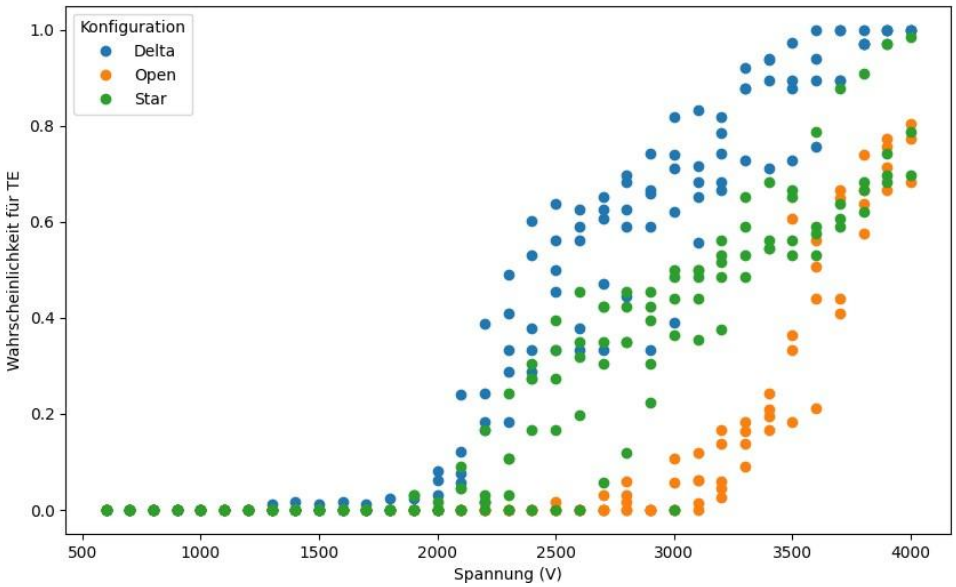

Figure 15: Probability of PD occurring when pulses of different voltages are applied, broken down according to the connection configuration.

The data presented show that the maximum overvoltage of 1.1 kV generated by the VSDs is well below the voltage range at which a significant increase in PD probability was observed. However, several points must be considered:

- **Pulse frequency effect:** Even a PD probability of only 1% would correspond to 160 PD events per second at an VSD PWM frequency of 16 kHz (the test frequency of both VSDs). SiC VSDs, however, can reach switching frequencies of up to 100 kHz, further amplifying this effect.
- **Temperature dependence:** The PD tests were carried out at room temperature, while the motor reaches up to 140 °C under full-load operation. The relationship between PD inception voltage and temperature is complex, but in general PDIV decreases with temperature. A value of approximately –4 V/K has been reported in the literature.
- **Slew rate and waveform differences:** The slew rate and voltage waveform of the VSDs differ from those of the laboratory test device. This can lead to variations in PD activity and must be considered when interpreting results.
- **Variability of PDIV/RPDIV:** PDIV and RPDIV values can vary greatly depending on the test method, in part due to differences in inception voltage between measurement configurations. This becomes even clearer when the sinusoidal voltage tests are discussed below.

For these reasons, PDIV and RPDIV values obtained in the laboratory should not be compared directly with the stresses occurring in operation. Instead, conclusions should be drawn only from changes in PDIV and RPDIV measured under consistent test conditions.

In addition, significant differences in PDIV can occur between otherwise identical motors. For example, motor “A” (operated with the SiC VSD) already exhibited significantly lower PD inception voltages in its brand-new condition compared to motor “B” (operated with the Si VSD). Figure 16 illustrates this: the probability of PD is plotted for both motors at the start of testing, with the 50% probability line highlighted in red to facilitate reading of the RPDIV. The

first PD was detected at 1.3 kV for motor “A,” whereas motor “B” did not exhibit PD until 2.0 kV. The repetitive PD inception voltages also differed markedly, ranging from 2.2–3.3 kV in the “Delta” configuration, 2.4–3.6 kV in “Star,” and 3.5–3.9 kV in the “Open” configuration.

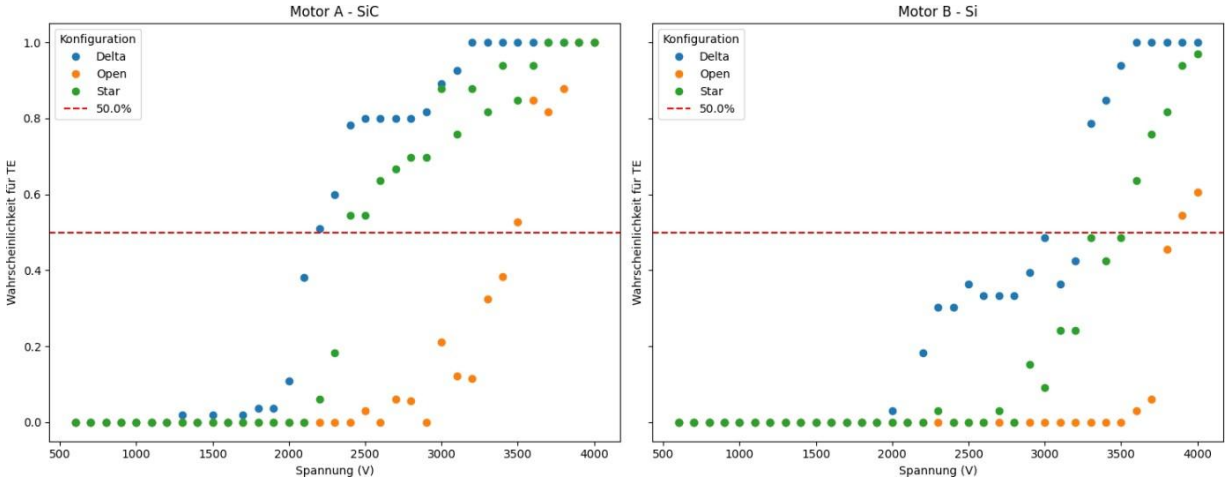

Figure 16: Probability of PD when applying pulses of different voltages for motor "A" with SiC VSD and motor "B" with Si VSD. Measurements with brand-new motor before the start of the long-term test.

Such large differences can also influence the future ageing behaviour of the insulation and are likely one of the main reasons why many ageing tests reported in the literature are not conducted on complete motors but rather on twisted-pair specimens of enamelled wire. Another contributing factor is the long test duration required before measurable differences in ageing can be observed.

8.4. Insulation test at mains frequency

The insulation test with sinusoidal voltage was analysed in less detail than the impulse-voltage test, resulting in a smaller dataset and less robust statistical analyses. Nevertheless, several important differences were observed.

Figure 17 shows the probability of PD as a function of the applied RMS voltage. A striking finding is the large difference between the PDIV determined under surge-voltage excitation and that determined with sinusoidal excitation. Under sinusoidal voltage, the first PDs were measured for motor *A* at 850 V (≈1.2 kVp) and for motor *B* at 920 V (≈1.3 kVp). In contrast, PDIV values obtained from surge-voltage tests were higher and exhibited greater variation between the two motors.

From a test voltage of about 1 kV (≈1.4 kVp) onward, PDs become very likely under sinusoidal excitation, whereas significantly higher voltages are required to trigger PDs under pulse-voltage testing. These differences can be explained by the stochastic nature of PD, the ignition delay, and the type of excitation voltage (unipolar for impulse testing versus bipolar for sinusoidal testing).

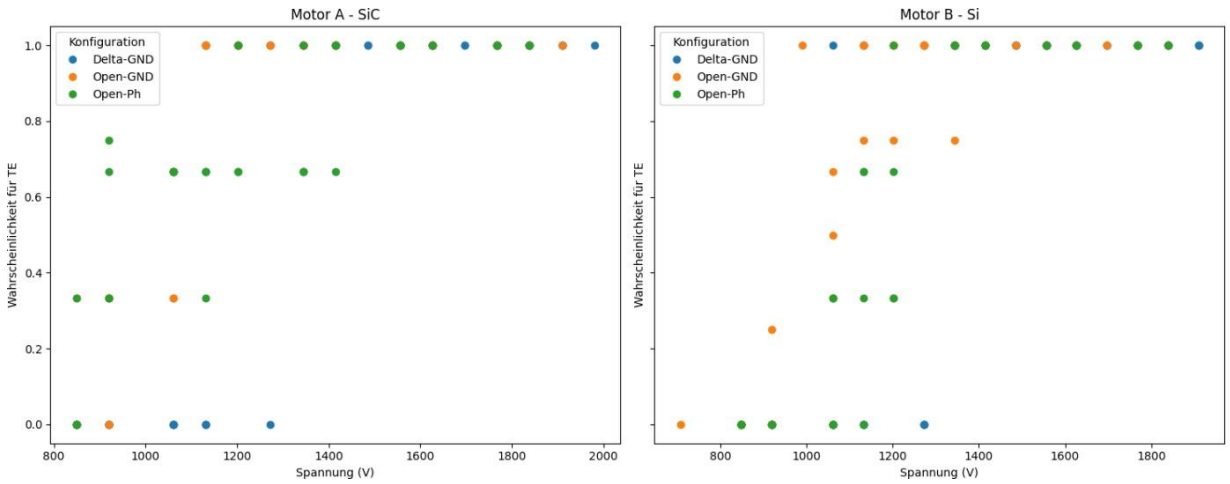

Figure 17: Probability of PD as a function of the test voltage for motor "A" operated with SiC VSD and motor "B" operated with Si VSD.

8.5. Ageing behaviour

The curve of RPDIV over the first 300 hours of motor running time, measured for both motors after 0, 50, 100, 200 and 300 hours, is shown in Figure 18.

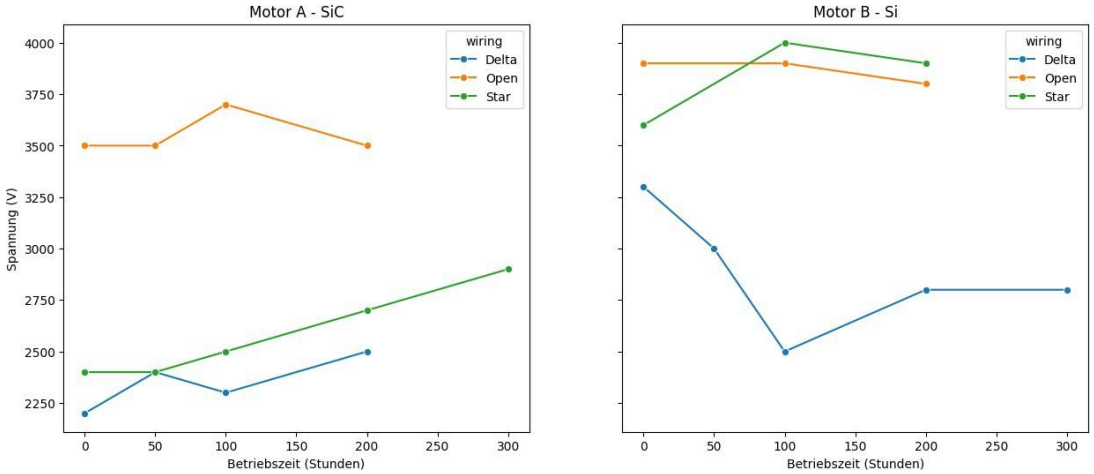

Figure 18: Time curve of the RPDIV of both motors measured for different measurement configurations.

The results obtained so far do not permit any well-founded conclusions regarding insulation ageing. On the one hand, the measurement period was too short; on the other, the data exhibited considerable variation. In general, it is unlikely that pronounced signs of ageing would appear after such a limited operating time. After 300 operating hours, only very few PD events were detected, preventing the determination of reliable RPDIV values. The cause of this remains unclear.

As noted earlier, three SiC VSDs failed during the tests, bringing the endurance study to a premature standstill. There is, however, interest in continuing these investigations in a follow-up project using a different SiC VSD.

9. Conclusions

Fast voltage rise times of 30 ns (SiC VSD) and 80 ns (Si VSD) were measured. With a 15 m cable, these transients produced motor overvoltages of up to 1.1 kV. The motor manufacturer ABB does not specify permissible overvoltage limits for such short rise times (Figure 19). However, several studies indicate that such steep voltage slopes can negatively impact insulation lifetime. This makes further investigation of the phenomenon highly relevant.

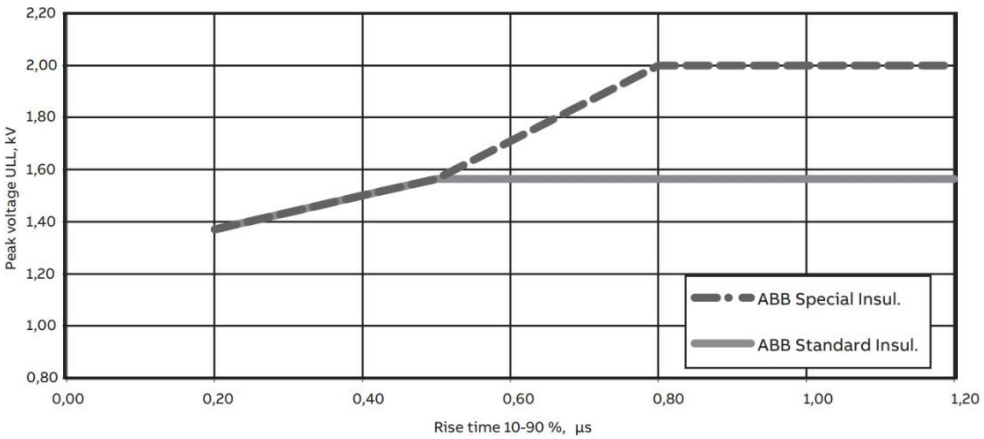

Figure 19: Permissible phase-to-phase voltage as a function of the rise time at the motor connection terminals[8]

Test methods in accordance with **DIN EN 60034-18-41** were applied to assess the insulation condition. It became clear that PDIV and RPDIV values can vary considerably depending on the measurement configuration. In the measurements carried out after 0, 50, 100, 200, and 300 operating hours, several configurations were used each time. For future work, however, it appears more expedient to focus on a single configuration—the one that has shown the strongest effects to date and offers the most comparative data from the literature. Concentrating on one setup will allow a greater number of measurements under identical conditions, thereby reducing statistical variation. The **"delta" configuration** is considered the most suitable for this purpose.

During the measurements, it was also observed that the PD inception voltages of the two motors differed significantly even in their brand-new state. Although this can be attributed to manufacturing tolerances, it may also influence future ageing behaviour under operation with the different VSDs, complicating the detection of clear ageing-related differences.

Furthermore, the repetitive PD inception voltage (RPDIV) obtained from impulse-voltage testing exhibited much larger variations than the PDIV obtained from withstand-voltage testing at mains frequency. Nevertheless, the impulse test is probably more suitable for detecting ageing differences, as its voltage waveform is closer to that of VSD operation.

Despite these insights, many questions remain unanswered—largely due to the short test duration of only 300 hours. This limitation was caused by repeated failures of the SiC VSD, which broke down three times during this period. As the manufacturer has not yet been able to determine the root cause, the test had to be discontinued.

[8] Catalogue ABB. IEC Low voltage Process performance Aluminium Motors, 11-2023

9.1. Bearing Currents

Currents flowing through the rolling bearings of electrical machines are referred to as **bearing currents**. In mains-powered motors, these were traditionally caused by magnetic asymmetries, among other factors. However, due to improvements in motor design and manufacturing, such classical bearing currents are now of limited relevance. Instead, bearing currents induced by the operation of motors with VSDs have become the primary concern.

Excessive bearing currents can locally melt the raceways, affecting the rolling of the elements, or chemically degrade the bearing grease. Both mechanisms lead to a reduced bearing lifetime and shorter maintenance intervals for the electrical machine.

9.2. Categorisation of bearing flows

There are essentially four types of bearing currents caused by the PWM operation of VSDs[9]:

1. **Capacitive dU/dt bearing currents**
2. **Electrical Discharge Machining (EDM) bearing currents**
3. **High-frequency circulating bearing currents**
4. **Rotor-to-earth bearing currents**

These are explained in more detail below.

Capacitive dU/dt bearing currents
The capacitive dU/dt bearing current arises from parasitic capacitances in electrical machines. These capacitances form a capacitive voltage divider, such that part of the common-mode voltage is coupled onto the shaft. The main capacitances involved are:

- C_{wwr} : stator winding-to-rotor capacitance
- C_{rf} : rotor-to-case capacitance
- $C_{b,DE}$ and $C_{b,NDE}$: bearing capacitances at the drive-end (DE) and non-drive-end (NDE)

The equivalent capacitances and their relationships are illustrated in Figure 20.

[9] H. Tischmacher, "System Analyses of the Electrical Load on Rolling Bearings in Inverter-Fed Electric Motors", Doctoral Thesis, Hannover : Gottfried Wilhelm Leibniz Universität Hannover, 2017 16
K. B. Tawfiq, M. Güleç, and P. Sergeant, "Bearing Current and Shaft Voltage in Electrical Machines: A Comprehensive Research Review", Machines, Vol. 11, No. 5, Art. No. 5, May 2023

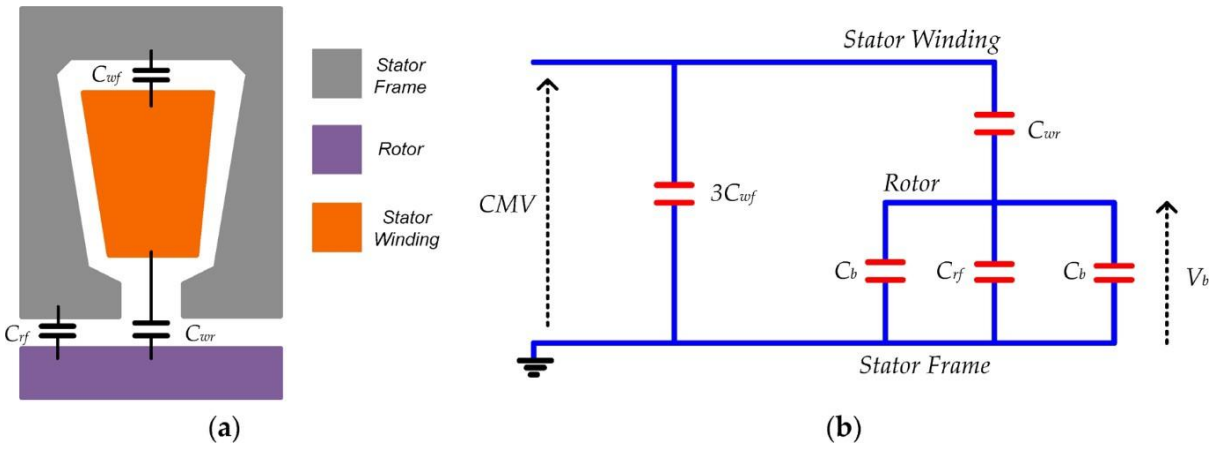

Figure 20: Equivalent circuit diagram of the parasitic capacitances in an electrical machine. [16]

Capacitive dU/dt storage currents

These currents are understood as the charging and discharging of the bearing capacitances $C_{b,DE}$ and $C_{b,NDE}$. For a bearing capacitance to exist, a fully insulating lubricating film is required. This condition is not fulfilled at low speeds (<100 rpm) or at standstill, where the bearing surfaces are in metallic contact and thus present a low-impedance resistance.

When an insulating lubricating film is present, the voltage across the bearing is typically in the range of 1–9% of the common-mode voltage and can be calculated as follows:

$$U_b = U_{CM} \frac{C_{wr}}{C_{wr} + C_{rf} + C_{b,NDE} + C_{b,DE}}$$

With the common-mode voltage U_{CM} calculated from the average of the phase voltages U_u, U_v, U_w.

$$U_{CM} = \frac{U_u + U_v + U_w}{3}$$

Each switching operation causes a change in the common-mode voltage, which in turn induces capacitive currents in the bearings. These currents are typically very small and are not considered harmful to either the bearings or the lubricant.

EDM bearing currents (Electric Discharge Machining, or spark erosion)

The same bearing voltage that causes capacitive dU/dt currents can also give rise to **EDM bearing currents** when the voltage exceeds the dielectric strength of the lubricating film. In this case, the bearing voltage U_b builds up to a maximum value determined by the insulating properties of the lubricant (composition, film thickness, temperature, etc.). Once this threshold is exceeded, the voltage collapses abruptly to zero as the bearing capacitances C_b and the rotor-to-frame capacitance C_{rf} discharge. This produces a short, high-current pulse that can reach several amperes before decaying. After the discharge, the bearing regains its insulating behaviour, and the voltage begins to build up again.

A typical EDM discharge current is illustrated in Figure 21. This type of bearing current is characterized by short, high-amplitude pulses with sufficient energy to locally melt or even vaporize sections of the bearing raceway. They are therefore considered highly damaging to

rolling bearings. The occurrence, frequency, and intensity of EDM discharges strongly depend on the operating conditions of the motor, including speed, lubricant type, and temperature..

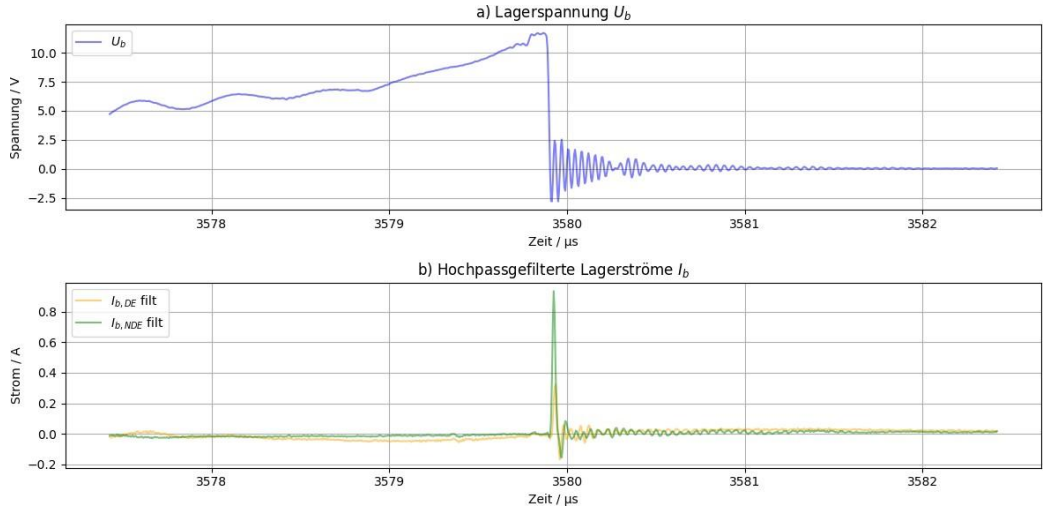

Figure 21: Typical course of the bearing voltage and the bearing current when discharge bearing currents (EDM bearing currents) occur.

High-frequency circulating bearing currents

During each switching operation, a current flows through the motor housing due to the parasitic capacitance between the winding and the stator laminated core, denoted as C_{wf} in Figure 20. This current is discharged via the earth or shield cable and generates a high-frequency magnetic flux encircling the motor shaft. The induced shaft voltage from this flux drives a **high frequency circulating current**, which closes its path through the laminated core, end shields, motor bearings, and shaft.

The capacitance C_{wf} increases with motor size, which is why circulating bearing currents were historically considered critical mainly in motors above 100 kW. However, with today's significantly faster voltage rise times, even smaller capacitances can produce substantial currents. As a result, high frequency circulating bearing currents have again become relevant for smaller machines and warrant closer investigation.

Rotor-to-earth bearing currents

Under normal conditions, most of the current coupled into the housing via the winding-to-stator capacitance is returned to the VSD through the earth or shield cable. However, if the load is earthed and a lower-impedance path exists via the end shields, through the motor bearings, the shaft, and into the load, a large **rotor-to-earth current** can flow. These currents are harmful not only to the motor bearings but especially to the bearings of the driven load.

Such currents can be largely mitigated by using insulated couplings and by ensuring proper earthing.

Summary

All types of bearing currents originate from parasitic capacitive coupling at the beginning of the current path. Since current through a capacitance depends on the rate of voltage change, it can be concluded that VSDs with faster rise times generate higher bearing currents.

9.3. Literature review

The following section summarises the results of three studies that explicitly analysed bearing currents in connection with SiC-based VSDs.

- **Study 1 – Initial comparison of SiC vs. Si VSDs**[10]

  In this study, the bearing currents of a 5 hp (3.7 kW) motor were measured using either a SiC VSD (rise time 48–50 ns) or a Si IGBT VSD (rise time 190 ns). The experiments showed that both the maximum bearing voltage and the measured bearing currents, as well as their frequency of occurrence, increased significantly when operated with the SiC VSD. Bearing currents were generally only observed after the motor had been running for 10–20 minutes; before this, the lubricating film in the bearing was too thick because the bearings were still cold. The authors focused their analysis exclusively on EDM bearing currents.

- **Study 2 – Extended analysis including modelling and temperature effects**[11]

  In a follow-up publication by the same authors, the bearing current measurements were extended with an electrical model and statistical analyses, with particular attention to the influence of temperature. The results showed that EDM currents rarely occur at low bearing temperatures (below 30 °C). The amplitudes of bearing currents and voltages reached their maximum for both VSDs at a bearing temperature of approximately 37 °C, with slightly higher values for the SiC VSD. At higher temperatures, both amplitudes decreased, but not equally: the SiC VSD still produced higher values in the range of 50–60 °C. The authors concluded that SiC VSDs impose higher electrical stress than Si VSDs, particularly in motors operating close to maximum load and thus running at elevated temperatures.

- **Study 3 – Influence of electrical and mechanical parameters**[12]

  In this investigation, the bearing currents of a 7.5 kW induction machine operated with a SiC VSD were measured. The effects of rise time, PWM frequency, DC-link voltage, and bearing temperature were analysed. The study found that although dU/dt bearing currents increased significantly with faster rise times, the number of particularly damaging EDM discharges per unit time remained unchanged. In contrast, PWM frequency, DC-link voltage, and temperature had a much stronger influence:

  - **PWM frequency:** EDM events increased linearly up to 60 kHz, then declined.
  - **DC-link voltage:** EDM currents rose exponentially with voltage.
  - **Temperature:** Few EDM events occurred below 25 °C, while a sharp increase was observed around 35 °C.
  - **Speed:** The number of EDM events was highest at 150 rpm, but their frequency dropped sharply at higher speeds.

[10] A. von Jouanne et al, "Motor Bearing Current Characterisation in SiC- based Variable Frequency Drive Applications," 2020 IEEE Energy Conversion Congress and Exposition (ECCE), Detroit, MI, USA, 2020, pp. 2718-2725

[11] R. Collin, A. Yokochi and A. v. Jouanne, "Novel Characterisation of Si- and SiC-based PWM In- verter Bearing Currents Using Probability Density Functions," 2021 IEEE Energy Conversion Con- ference and Exposition (ECCE), Vancouver, BC, Canada, 2021, pp. 5146-5153

[12] R. Collin, A. Yokochi and A. v. Jouanne, "Novel Characterisation of Si- and SiC-based PWM In- verter Bearing Currents Using Probability Density Functions," 2021 IEEE Energy Conversion Con- ference and Exposition (ECCE), Vancouver, BC, Canada, 2021, pp. 5146-5153

9.4. Own measurement results

The results of the bearing current measurements exhibit characteristic features that are not specific to the VSD, but are primarily influenced by the measuring device, the motor, and the installed bearings. For this reason, a complete interpretation of the measurement results obtained with the Lenze i550 (Si-based) VSD is presented first. The specific differences between the Si- and SiC-based VSDs are discussed afterwards.

Operation at rated speed

Figure 22a shows the bearing currents at the drive end (DE) and non-drive end (NDE) when the motor was operated at 50 Hz with the Lenze VSD under no-load conditions. Both bearing current signals are superimposed by a dominant component at the motor's fundamental frequency (50 Hz, 20 ms period). This component does not represent a real current flow in the shaft or bearings but is instead an interference signal caused by electromagnetic coupling from the stator winding currents to the Rogowski coils positioned nearby.

To eliminate this effect, a high-pass filtered version of the signals is typically used for further evaluation, as shown in Figure 22b (denoted with the suffix "filt"). The high-pass filtered DE bearing current ($I_{b,DE}$) shows a high-frequency signal with an amplitude of approximately 0.1 A_p, with isolated peaks reaching up to 0.2 A_p. The NDE bearing current ($I_{b,NDE}$) exhibits a slightly higher overall amplitude, but no distinct current peaks.

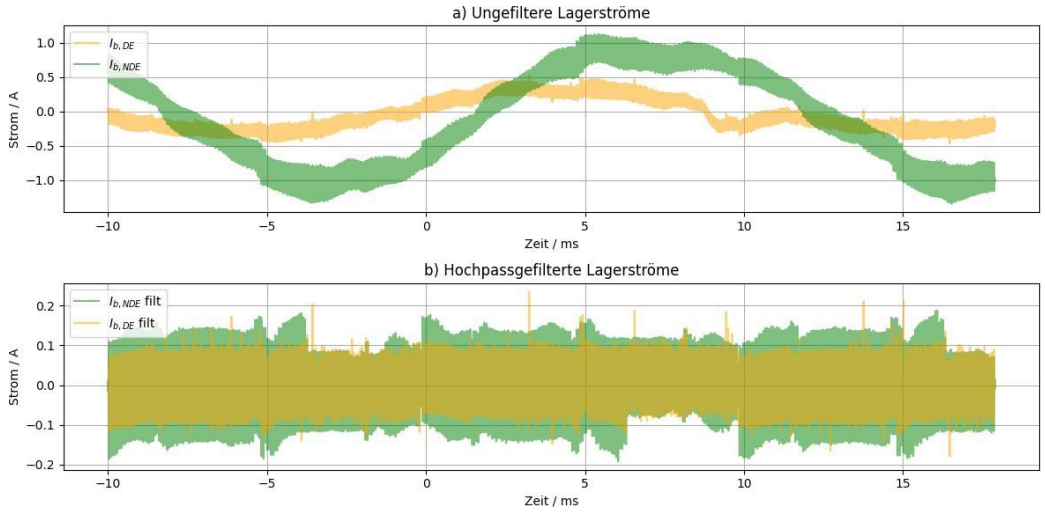

Figure 22: The measurements of the Rogowski coil are superimposed by an interference signal (a). High-pass filtering makes it possible to measure the real bearing current (b).

Figure 23 shows the bearing voltage and the common-mode voltage in (a), and the filtered load currents in (b). The common-mode voltage does not appear as discrete steps (-Udc, -1/3 Udc, 1/3 Udc, …) because the high switching frequency of 16 kHz combined with the long motor supply cables causes reflections and superpositions. As a result, the waveform appears strongly smoothed.

The bearing voltage remains at 0 V for most of the time but exhibits oscillations at every switching event, which are also visible in the bearing current signals. Occasionally, the bearing voltage can be seen to "follow" the common-mode voltage. This indicates that the

lubricating film acts as an insulator, allowing the capacitive voltage divider described in Chapter 9.2 to transfer part of the common-mode voltage onto the shaft. However, even at relatively low bearing voltages this condition breaks down, and the bearing transitions into a resistive state.

Such breakdowns of the lubricating film's insulating properties can occasionally result in small discharge current peaks (EDM currents), as illustrated in Figure 23 at approximately 0.05 ms. Owing to the low breakdown voltage, the stored energy is minimal, and the resulting EDM current is very small—generally much smaller than the currents associated with the switching cycles. According to both the literature and previous measurement results from other authors, such low-amplitude EDM currents are not considered harmful.

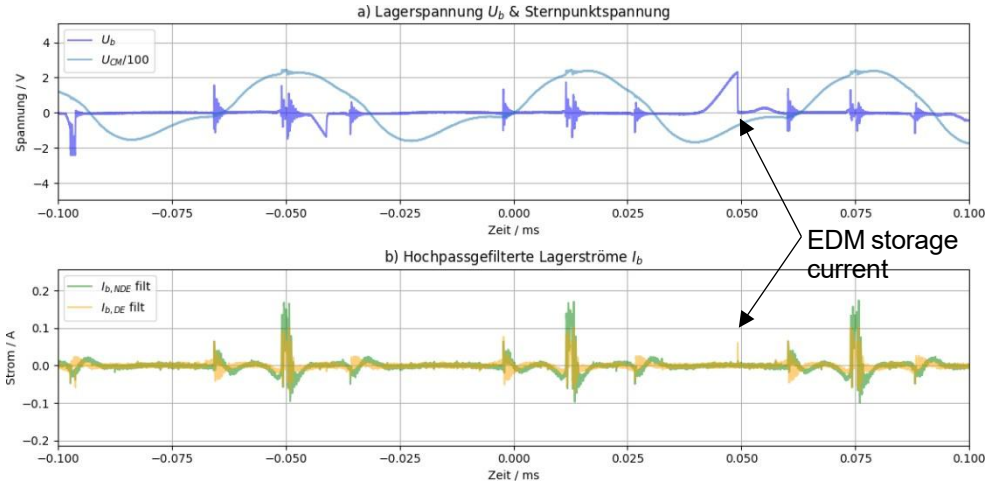

Figure 23: Curve of the common-mode voltage and bearing voltage in a) and the filtered bearing currents in b).

These observations correspond to the classification scheme shown in Figure 24. According to this categorisation, most of the measurements fall into the **"C: Resistive currents / No EDMs"** range. In this state, the lubricating film is sufficiently thin—due to elevated temperature and high operating speed—that either metallic contact occurs in the bearing or the voltage amplitudes are high enough for the insulating properties of the film to become negligible.

According to several studies, a similar effect is expected when conductive greases are used. However, in agreement with the motor manufacturer ABB, no conductive grease was applied in the motors examined here.

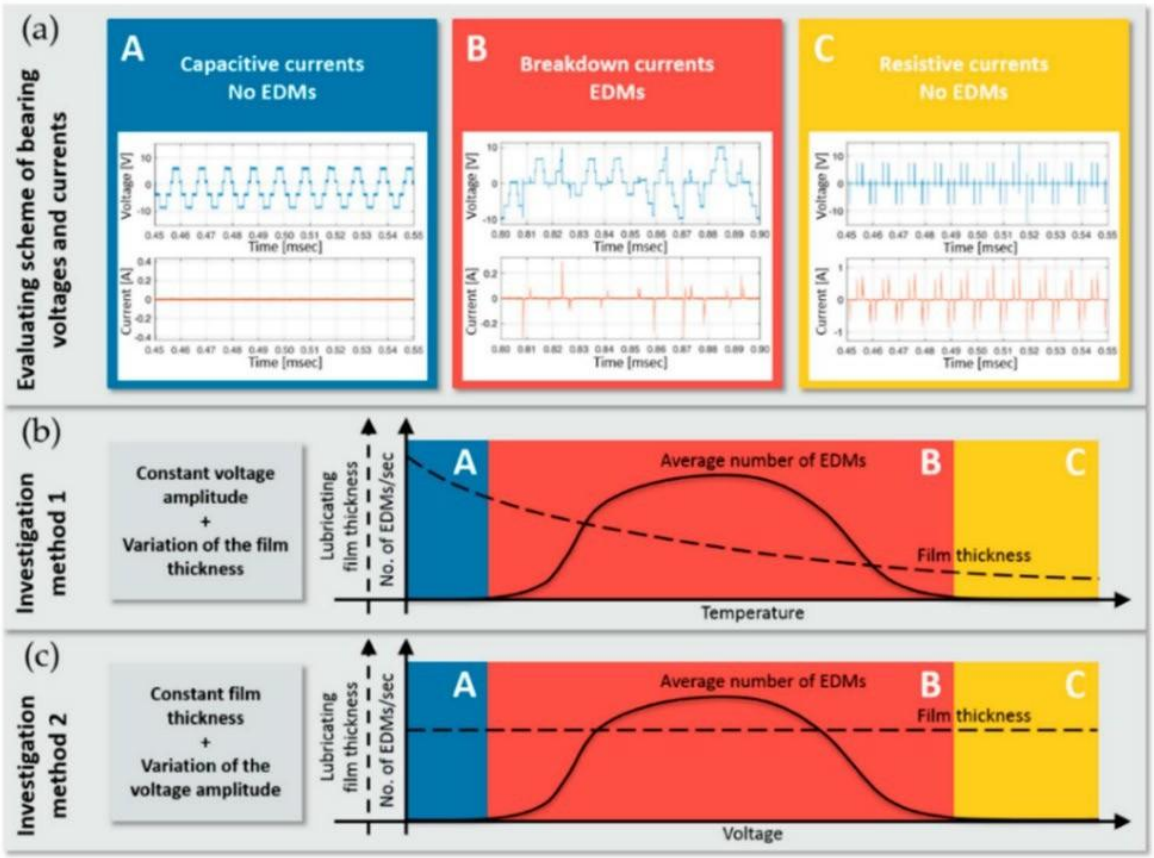

Figure 24: Categorisation of bearing currents into three types. The differences result primarily from the insulating properties of the lubricating film, which depend on its thickness (temperature, speed).

Special case: Cold bearing

A significant increase in the number and intensity of EDM discharges was observed during motor start-up at room temperature or during rotor acceleration. In the measurement shown in Figure 25, for example, ten current peaks with amplitudes greater than 0.5 A were detected within a 10 ms interval. This behaviour can be explained by the thicker lubricating film at reduced temperatures, which allows the bearing voltage to rise to higher values before breakdown occurs. In this case, the bearing voltage reached 12 V and the EDM current peaked at 1.25 A.

The increase in EDM activity at low temperatures was observed for both the Si- and SiC-based VSDs. However, after only 15 minutes of operation at nominal speed, EDM events became very rare, and their amplitudes fell well below 0.5 A. Consequently, motors that are operated permanently at low temperatures, or those subject to frequent start–stop cycles, experience significantly higher bearing stress from EDM currents than motors operated continuously at room temperature under steady speed and load.

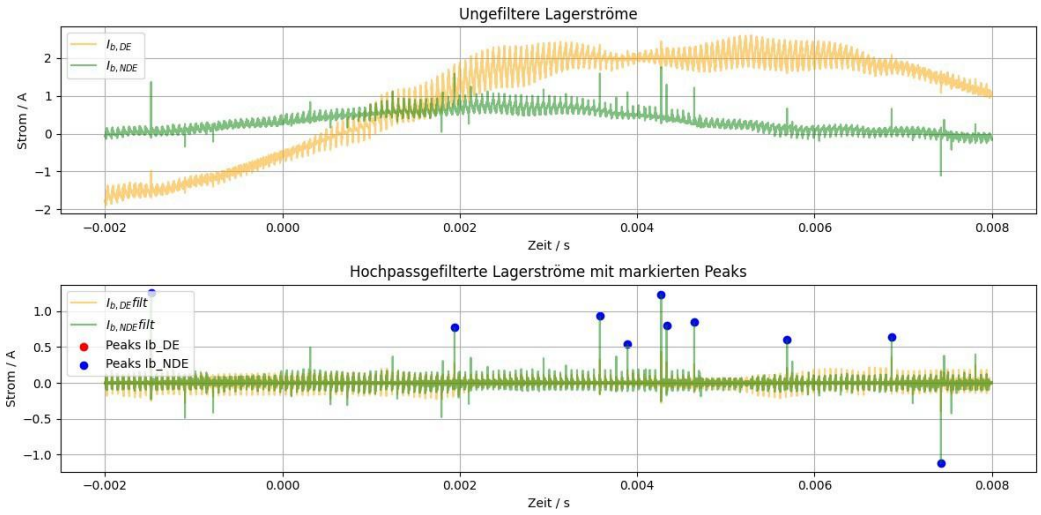

Figure 25: Bearing currents at temperatures of approx. 25 °C. At these temperatures, the lubricant film is thicker and a build-up of stress over the bearing is possible. This results in high EDM bearing currents.

Special case: Low speeds

Particularly high bearing currents were observed at low speeds between 0 and 100 rpm. Figure 26 shows the bearing voltage and one of the phase voltages in (a), and the bearing currents together with the earth current in (b), for operation with the Lenze VSD at 60 rpm. At such low speeds and under no-load conditions, the modulation index is very small and the phases switch almost simultaneously. This results in large common-mode currents (stator earth current I_{sg}) of up to 10 $A_{p.}$

At the same time, the bearings are in metallic contact at low speeds, since the rolling elements are not supported by a lubricating film. This combination leads to large circular currents of around 2 $A_{p.}$. However, because the contact is ohmic and the effective contact area is relatively large at low speeds, these bearing currents are currently assumed not to be harmful.

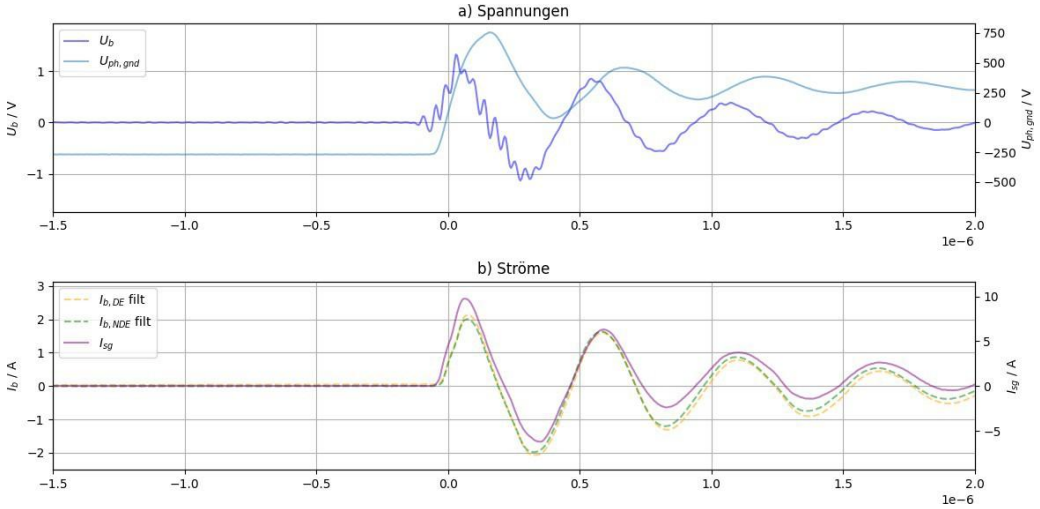

Figure 26: Layer currents at a speed of 60 rpm using the Lenze VSD

When using the LARA-100k VSD (Figure 27), earth currents of up to 22 A_p were measured at low speeds—more than twice the value observed with the Lenze VSD. This increase can be attributed to the stator winding–to-laminated core capacitance (C_{wf}) inherent to the motor, combined with the higher slew rate of the SiC VSD (18 kV/µs compared to approximately 7 kV/µs for the Lenze). These higher earth currents also resulted in significantly larger circulating currents, reaching up to 5 A_p.

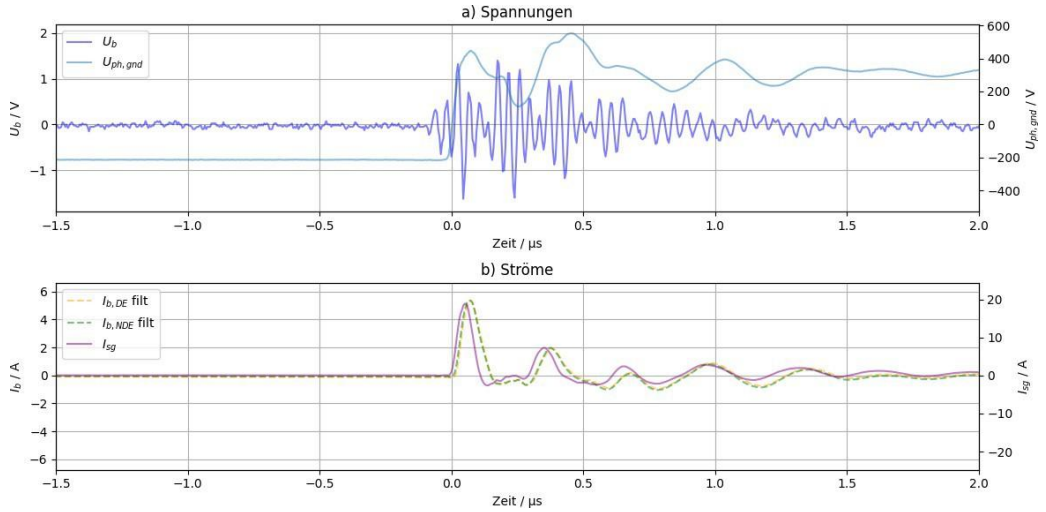

Figure 27: Load currents at standstill using the LARA-100k VSD

Currents during switching cycles at rated speed

At nominal speed and operating temperature, the tested motor showed neither a direct image of the common-mode voltage in the bearing voltage nor significant EDM currents. Instead, the bearings were predominantly in an ohmic state. According to Figure 28, which classifies different bearing current behaviours as a function of temperature and lubricant film thickness, the tested motor therefore corresponds to **“state 5”** when operated with both the LARA-100k and the Lenze VSD.

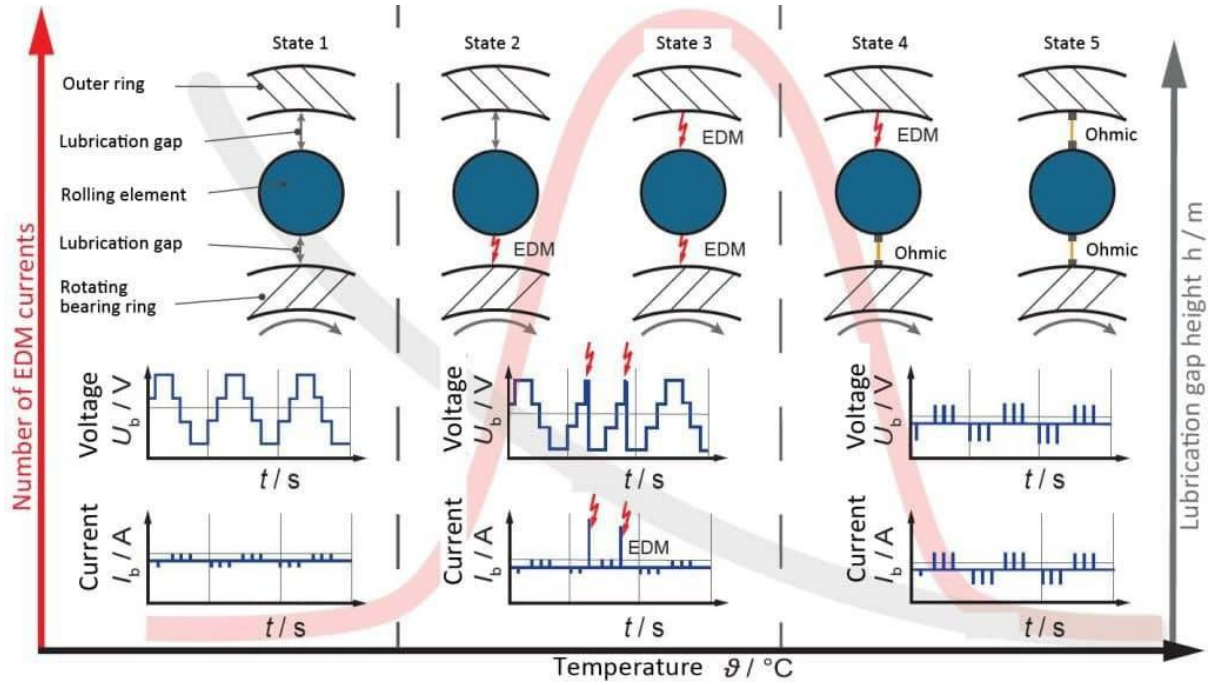

Figure 28: Classification of bearing current behaviour according to temperature and lubricant film thickness[13].

In this operating state, the bearing voltage and bearing currents are characterised by small peaks occurring with each switching operation. Although the peaks are relatively small, their amplitude increased significantly when the motor was operated with the SiC VSD compared to the Si VSD, as shown in Figure 29. Figures a) and b) present measurements with the Lenze VSD, while Figures c) and d) show results with the LARA-100k VSD.

With the Lenze VSD, the number of peaks is lower because the device employs overmodulation at 50 Hz. In this mode, one of the phases remains constant at +Vdc or –Vdc for a certain interval rather than switching, thereby reducing the number of switching operations. The maximum amplitude of the bearing currents differs by approximately a factor of two between the two VSDs. However, the damaging influence on bearings is likely determined not only by the maximum amplitude but also by the frequency of occurrence. Consequently, the SiC VSD—with more switching operations and consistently higher bearing current amplitudes—can be expected to exert a considerably stronger negative impact on bearing lifetime.

The driving mechanism for these bearing currents is the stator earth current I_{sg}, which induces circular bearing currents, as discussed earlier for the special case of low speeds. Compared to low-speed operation, the stator earth current is significantly reduced at nominal speed, since the modulation index increases and the common-mode currents no longer overlap additively. Nevertheless, the stator earth current remains higher with the SiC VSD than with the Si VSD at all speeds, leading to correspondingly higher circular bearing currents.

[13] https://flucon.de/en/fluid-lexicon/breakdown-currents-in-rolling-bearings/

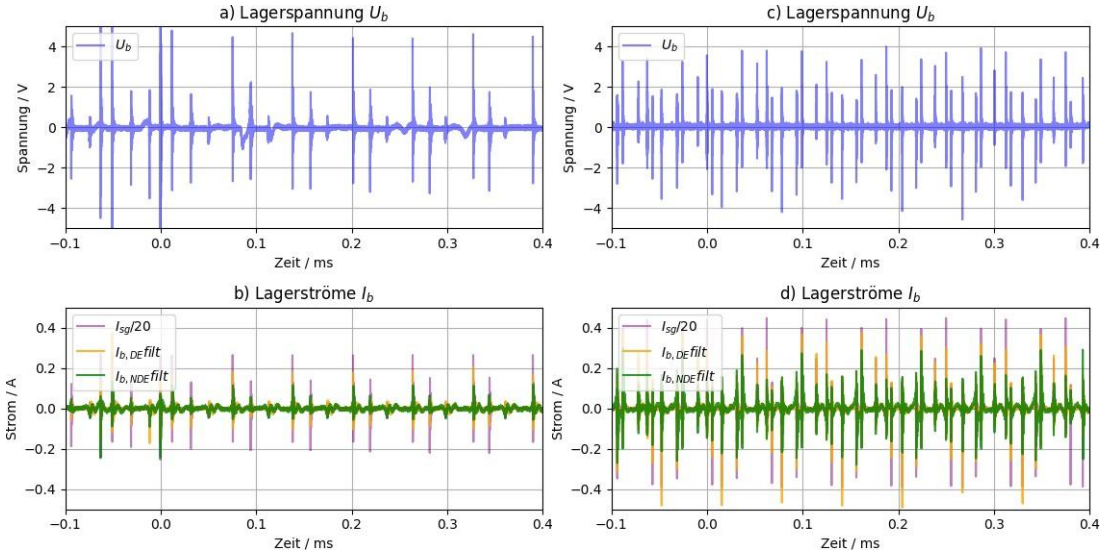

Figure 29: Comparison of the bearing voltages and bearing currents between Si in a) and b) and SiC in c) and d). The motor was operated in each case at 50 Hz and without load and has warmed up to operating temperature.

9.5. Conclusions

The EDM bearing currents—often categorised as the most damaging of the bearing current types—were not observed in the tested machine at nominal speed and operating temperature, regardless of whether the motor was supplied by the Si- or SiC-based VSD. Instead, the bearings were in a resistive state, characterised by a very thin lubricant film. In this state, bearing currents occur during each switching event, but no voltage build-up across the bearings takes place, which is a prerequisite for EDM discharges.

There are isolated indications that the fast rise times of the common-mode voltage tend to promote breakdown of the lubricating film, thereby preventing a bearing voltage build-up. From this perspective, the faster rise times and higher switching frequencies of SiC VSDs could even be advantageous—if only EDM bearing currents are considered.

However, a direct consequence of faster slew rates is an increase in common-mode currents. These currents, normally conducted via the motor housing and earth/shield cable in the resistive state, also drive high-frequency circular bearing currents. Such currents were found to be significantly more pronounced with SiC VSDs compared to Si VSDs. Whether the measured amplitudes are already sufficient to cause bearing damage would require long-term endurance testing and subsequent bearing inspection.

Low-impedance earthing is therefore of particular importance, ensuring that common-mode currents do not develop into harmful rotor-to-earth currents, which would impose additional stress on both motor and load bearings. While this requirement applies to all VSDs, the measured common-mode currents with SiC technology were more than double those of the Si VSD, depending on the operating state. This underlines the need for particular care in the selection of cabling and earthing concepts when operating motors with SiC VSDs.

The mitigation measures commonly applied to reduce bearing currents—such as insulated bearings, common-mode chokes, or shaft earthing brushes—were not investigated in this study. Nevertheless, it can be assumed that these established methods are also effective when applied to SiC VSDs.

These results —particularly the behaviour of the EDM currents— deviate from the findings reported in the literature but can be explained using the classification schemes for EDM currents. While the motors described in the literature typically fall into the **“Capacitive Currents / No EDM”** range at room temperature, the motor analysed in this study was already in the **endangered range** at room temperature, where EDM currents occur. As the temperature increases, the lubricating film becomes thinner and both motors transition into the next range.

This demonstrates that bearing current behaviour strongly depends on the specific motor, the bearing design, the lubricant used, and the operating temperature. Consequently, analysing the VSD alone is not sufficient to assess bearing current risks.

10. Wide Bandgap Power Semiconductor Industrial VSD Research Roadmap 2024-2027

The following research topics were identified for the **research roadmap** at the workshop on 15 May 2024:

- **High initial costs**
  - Cost comparison at the component level with estimated production costs.
  - Cost comparison at the system level based on total cost of ownership (TCO) for different utilisation cycles.
  - Cost comparison on a holistic level using life-cycle assessment (LCA) for environmental impact and circular economy considerations.
- **Application maturity**
  - This topic must be coordinated with PECTA. PECTA's annual reports will be integrated into the White Paper.
  - The most important contributions will address:
    - Production capacity and availability
    - Supply chain challenges
- **Design and implementation: Topologies**
  - Comparison of multilevel topologies using WBG power semiconductors with conventional Si-based two-level VSDs, focusing on efficiency and volume.
  - Evaluation of alternative topologies enabled by WBG devices (e.g., current-DC link VSDs, flying-capacitor multilevel VSDs, sparse neutral-point-clamped VSDs), with emphasis on efficiency and performance.
- **Design and realisation: Auxiliary facilities**
  - This topic was dropped, as it was deemed less fundamental than "topologies" and less application-oriented than "operating parameters" or "filters." Consideration of novel gate-driver or auxiliary power-supply topologies was judged too detailed for the core content of the White Book.
- **Design and implementation: Filters**
  - Special considerations for the design and proper dimensioning of input filters for multilevel GaN-based active front-ends.
  - Requirements and performance of full-sine output filters and motor-side EMI filters (including radiated emissions).
- **Design and implementation: Operating parameters**
  - Optimisation of operating parameters for maximum efficiency, including standard, multilevel, and dual open-winding topologies. Parameters to be considered include switching frequency, switching speed, filter dimensioning, and thermal behaviour (both software- and hardware-related).
  - Analysis of specific effects such as dynamic on-resistance in GaN or residual soft-switching losses in SiC.

- **Aspects of reliability and durability**
    - State of the art in mean-time-between-failure (MTBF) prediction for WBG semiconductors, including comparison of power cycling behaviour between WBG and IGBT devices.
    - Advances in reliability modelling for WBG semiconductors.
    - Standard technologies for thermal optimisation, e.g., Z_{th} characterisation of WBG devices, including thermal cross-coupling between chips in a module.
    - Advanced thermal optimisation approaches, such as high-accuracy thermal monitoring (e.g., online junction temperature measurement via optical fibres or integrated gate drivers).
- **Risks and equipment requirements**
    - Effects of WBG industrial VSDs on bearings and insulation systems.
    - Implications of WBG VSD operation for EMC testing and required mitigation measures.
    - Increased accuracy and bandwidth requirements of measuring devices for testing WBG VSDs.

A **graphic on the next page** summarises and illustrates these research topics and their associated keywords.

Wide Bandgap Industrial Inverter Research Roadmap 2024-2027

Research Questions	Themes
RQ1: Application Readiness	• Cost comparison on component level • Cost comparison on system level • Cost comparison on holistic level • Production capacity and availability • Supply chain challenges
RQ2: Design and Implementation	• Comparison of WBG multilevel topologies • Potential of alternative topologies • Requirements and design of input and output filter design and topologies • Operational parameter optimization for optimal efficiency
RQ3: Reliability and Durability	• State of the art prediction of MTBF • Methods for WBG Reliability and Duration Testing • Advances in modelling of WBG power semiconductor • Standard and advanced thermal optimization technologies for WBG power semiconductors
RQ4: Risks to Equipment	• Impact on bearings and insulation aging • Impact on EMC Testing and EMC measures • Increased measurement equipment accuracy for WBG inverter testing

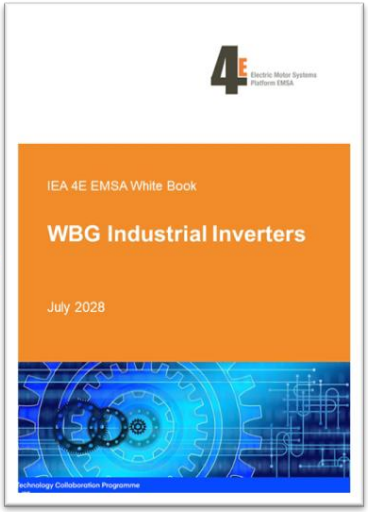

Electric Motor Systems
Platform EMSA

11. Conclusions

- **Efficiency potential:**

  Silicon carbide VSDs can improve overall efficiency by enabling higher switching speeds, which reduce motor losses. However, the switching frequency must be carefully matched to the motor. Excessively high switching frequencies increase VSD switching losses and can ultimately reduce overall system efficiency.

- **Filter design:**

  Higher switching frequencies allow for smaller input and output filters with reduced losses. This enables the design of more compact VSDs with high efficiency.

- **Insulation and bearing effects:**

  The fast voltage rise times of SiC VSDs cause increased overvoltages at the motor terminals. This must be carefully considered when retrofitting older motors whose insulation systems are not designed for such stresses. An increase in bearing currents has also been observed, although their harmfulness strongly depends on bearing type and operating temperature. A generalised assessment is therefore not possible.

12. Outlook and future implementation

The long-term test to compare insulation ageing could not be completed due to recurring problems with the SiC VSD. However, the construction of the test facility and the development of appropriate measurement methods have established a solid basis for demonstrating potential differences in insulation ageing, should they exist. It would therefore be highly desirable to continue the long-term test with an alternative SiC VSD in the framework of a follow-up project.

13. References

[1] IEC 61800-9-2 Adjustable speed electrical power drive systems - Part 9-2: Ecodesign for power drive systems, motor starters, power electronics and their driven applications - Energy efficiency indicators for power drive systems and motor starters

[2] RR'C Phase 2 V6_20190911.pdf: Guide to Round Robin Converter Losses (RR'C): Phase 2

[3] RR'C-Phase 2 Requirements-Labs.pdf: Round Robin Converter Phase 2: Requirements, Duties and Obligations of participating laboratories

[4] UTP 2.0 - 20190601.pdf: Converter loss measurement utilising a merge of the existing testing procedure in IEC 61800-9-2 and the experience gained from RR'C Phase 1, UTP 1.0

[5] UTP 2.0 - Supplemental paper 20191003.pdf: RR'C2, UTP 2.0 - Updated order of points

[6] Weijun Yin. Failure mechanism of winding insulations in inverter-fed motors. IEEE Electrical Insulation Magazine, 13(6):18-23, 1997

[7] Peng Wang, Andrea Cavallini, and Gian Carlo Montanari. The effects of square wave voltage rise time on pd statistics in time and frequency domain. In 2015 IEEE Electrical Insulation Conference (EIC), pages 262-265, 2015

[8] Kohei Shirabe, Mahesh Swamy, Jun-Koo Kang, Masaki Hisatsune, Yifeng Wu, Don Kebort, and Jim Honea. Advantages of high frequency PWM in AC motor drive applications. In 2012 IEEE Energy Conversion Congress and Exposition (ECCE), pages 2977-2984, 2012

[9] Lucien Porta, Andrea Vezzini. Implementation of electrical machine ageing testing. Bern University of Applied Sciences, 14 December 2022

[10] Shan Yin, King Jet Tseng, Rejeki Simanjorang, Yong Liu, and Josep Pou. A 50-kW High-Frequency and High-Efficiency SiC Voltage Source Inverter for More Electric Aircraft. IEEE TRANSACTIONS ON INDUSTRIAL ELECTRONICS, 64(11), 2017

[11] R. J. Kerkman, D. Leggate, D. Schlegel and G. Skibinski, "PWM inverters and their influence on motor overvoltage," Proceedings of APEC 97 - Applied Power Electronics Conference, Atlanta, GA, USA, 1997, pp. 103-113 vol.1, doi: 10.1109/APEC.1997.581440.

[12] S. Sundeep, J. Wang, A. Griffo and F. Alvarez-Gonzalez, "Antiresonance Phenomenon and Peak Voltage Stress Within PWM Inverter Fed Stator Winding," in IEEE Transactions on Industrial Electronics, vol. 68, no. 12, pp. 11826-11836, Dec. 2021

[13] D. Hewitt, S. Sundeep, J. Wang, A. Griffo, M. Diab and X. Yuan, "An Experimental Assessment of the Impact of High dv/dt SiC Converters on Insulation Lifetime of Electrical Machines," 2022 IEEE Energy Conversion Congress and Exposition (ECCE), Detroit, MI, USA, 2022, pp. 1-8

[14] P. Wang, A. Cavallini and G. C. Montanari, "The influence of repetitive square wave voltage parameters on enamelled wire endurance," in IEEE Transactions on Dielectrics and Electrical Insulation, vol. 21, no. 3, pp. 1276-1284, June 2014

[15] R. J. Kerkman, D. Leggate, D. Schlegel and G. Skibinski, "PWM inverters and their influence on motor overvoltage," Proceedings of APEC 97 - Applied Power Electronics Conference, Atlanta, GA, USA, 1997, pp. 103-113 vol.1

[16] H. Tischmacher, "System analyses of the electrical load on rolling bearings in inverter-fed electric motors", Doctoral thesis, Hanover : Gottfried Wilhelm Leibniz

Universität Hannover, 2017

[17] K. B. Tawfiq, M. Güleç, and P. Sergeant, "Bearing Current and Shaft Voltage in Electrical Machines: A Comprehensive Research Review," Machines, vol. 11, no. 5, art. No. 5, May 2023

[18] M. Weicker, "Common mode effects in inverter-fed electric motors", Ph.D. Thesis, Technische Universität, Darmstadt, 2021. doi: 10.26083/tuprints-00019145

[19] A. von Jouanne et al, "Motor Bearing Current Characterisation in SiC- based Variable Frequency Drive Applications," 2020 IEEE Energy Conversion Congress and Exposition (ECCE), Detroit, MI, USA, 2020, pp. 2718-2725

[20] R. Collin, A. Yokochi and A. v. Jouanne, "Novel Characterisation of Si- and SiC-based PWM Inverter Bearing Currents Using Probability Density Functions," 2021 IEEE Energy Conversion Congress and Exposition (ECCE), Vancouver, BC, Canada, 2021, pp. 5146-5153

[21] Y. Xu, Y. Liang, X. Yuan, X. Wu and Y. Li, "Experimental Assessment of High Frequency Bearing Currents in an Induction Motor Driven by a SiC Inverter," in IEEE Access, vol. 9, pp. 40540- 40549, 2021

[22] Puchtler, Steffen, Robert Maier, Martin Kuhn, and Yves Burkhardt. 2024. "The Influence of Load and Speed on the Initial Breakdown of Rolling Bearings Exposed to Electrical Currents" Lubricants 12, no. 1: 1.

[23] Andrea Vezzini, Sandie B. Nielsen: " Report on Round Robin of Converter Losses Final Report of Results" November 2022